Chemical Reviews

Volume 86, Number 4 August 1986

Structural and Magnetic Properties of Transition Metal Complexes of Pyridine *N*-Oxide

RICHARD L. CARLIN*

Department of Chemistry, University of Illinois at Chicago, Chicago, Illinois 60680

L. J. DE JONGH

Kamerlingh Onnes Laboratory, State University of Leiden, 2300RA Leiden, The Netherlands

Received February 27, 1986

Contents

I. Introduction

A small number of crystal lattices has been particularly important in the history of magnetic and other solid state investigations.[1] There is the cubic perovskite lattice, for example, noted for the isotropic compounds $KNiF_3$ and $RbMnF_3$, as well as the tetragonal lattice of K_2NiF_4; these particular structures have been important because they provide excellent examples of simple cubic (s.c.) and of 2-dimensional (2-D) antiferromagnets, respectively. The rutile structure (of MnF_2, FeF_2, etc.) forms another well-known crystal matrix for magnetic model systems. The series of compounds $(C_nH_{2n+1}NH_3)_2MCl_4$ (n = 1, 2 ...; M = Mn^{2+}, Cu^{2+}, Fe^{2+}) has yielded highly ideal 2-D magnetic systems, and in addition is intensively studied because of the interesting structural phase transitions that occur in these materials. The antifluorite structure exhibited by such substances as K_2ReCl_6 has also been studied extensively for the structural phase transitions which these compounds undergo. Finally, the family of AMX_3 compounds, e.g., $CsNiF_3$, $RbFeCl_3$, $[(CH_3)_4N]MnCl_3$, as well as the $MCl_2(py)_2$ series where M^{2+} is a 3d metal ion, have provided us with excellent examples of quasi-one-dimensional magnetic systems.

In the last few years we have been involved in a fairly extensive series of investigations on a new lattice system which has furnished in its own way a striking series of magnetic model systems of great diversity and novelty. The compounds are of the divalent iron series ions with the ligand pyridine *N*-oxide, C_5H_5NO. They are of the stoichiometry $[M(C_5H_5NO)_6]X_2$, where M may be manganese, iron, cobalt, nickel, copper, or zinc, and the anion X^- may be perchlorate, fluoborate, nitrate, bromate, or iodide. Donation by the pyridine *N*-oxide always occurs through the oxygen, and the molecule generally functions as a simple, monodentate ligand; there are in addition some compounds, especially with copper(II), in which the ligand forms a bridge between two metal ions. One of the notable chemical features of the ligand is that it tends to form complexes with the maximum coordination number of the particular metal, especially in the presence of weakly coordinating anions such as perchlorate or fluoborate. Several other compounds have been studied which involve a substituted pyridine *N*-oxide. This is found to change the crystal lattice structure profoundly, which is accompanied in turn by dramatic changes in the magnetic properties.

In this article, we review a number of the physical investigations on some of the pyridine *N*-oxide complexes, paying particular attention to the magnetic ordering phenomena which have been observed at low

0009-2665/86/0786-0659$06.50/0

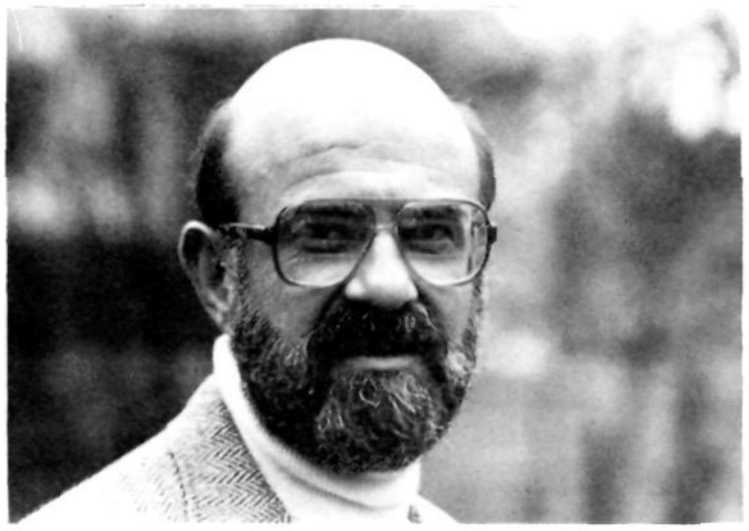

Richard L. Carlin, a professor of chemistry at the University of Illinois at Chicago, received his bachelor's degree from Brown University and his doctorate at the University of Illinois at Champaign-Urbana. He taught first at Brown, and has been in Chicago since 1967. His sabbatical leave in Leiden during 1973–1974 led to the work reported here, as well as the long-standing collaboration with his coauthor. His publications include the recent text entitled *Magnetochemistry*.

L. J. de Jongh studied experimental physics at the University of Amsterdam, where in 1974 he obtained his doctorate under the supervision of Prof. A. R. Miedema. His thesis concerned the study of magnetic model systems of low dimensionality. He has been a member of the permanent staff of the Kamerlingh Onnes Laboratory of the University of Leiden since then. His research is in low-temperature solid state physics, with emphasis on low-dimensional magnetic systems, solitons, low-dimensional synthetic conductors, metal cluster compounds, and intermetallic rare earth compounds.

temperatures. The $[M(C_5H_5NO)_6]X_2$ series of compounds has proved to be a rich source of information on some novel magnetic phenomena of fundamental interest to physics and magnetochemistry. It is also true that the investigations on these materials to date are limited by and large to structural crystallography, EPR studies, and magnetic susceptibility and specific heat measurements. Field-dependent studies, neutron scattering, NMR, and a variety of other measurements remain to be carried out. From the point of view of the rapidly developing field of magnetochemistry, these compounds provide some nice examples of magneto-structural correlations.[2]

The principal structural features of this system are the following:

1. The metal ions are 9.5 Å or more apart. This forces all observable cooperative magnetic phenomena to occur in the temperature interval below 1 K. This in fact turns out to be advantageous for then, for example, the lattice specific heat is essentially zero over the temperature region of interest, leaving the magnetic contribution to be measured directly. The low strengths of the antiferromagnetic exchange interactions in these materials allow field-dependent studies in easily accessible low fields (1–10 tesla).

2. All the compounds are isomorphous and belong to the same rhombohedral space group.

3. The compounds all have nearly equal unit cell lattice dimensions, and often are mutually miscible over all concentration ranges.

Of the novel magnetic phenomena encountered we mention in particular the first examples of the simple cubic XY model of magnetism, found in the cobalt(II) compounds, the field-induced magnetic ordering phenomena in $S = 1$ singlet-ground-state systems observed in the nickel compounds, and the ferro- and antiferrodistortive cooperative Jahn–Teller ordering in the copper compounds. The latter yield in fact the first experimental example of the 2-D Heisenberg antiferromagnet with spin $S = {}^1/_2$. Furthermore, the iron(II) compounds provide excellent examples of the Ising model in three spatial dimensions.

The isomorphic nature and mutual miscibility of these materials is another point of interest for the experimental physicist. This is because the compounds provide a crystalline matrix at the lattice nodes of which one may place, e.g., a random mixture of magnetic and nonmagnetic atoms, or equivalently of magnetic atoms of a different kind. The former case corresponds to the magnetic dilution problem, which in turn is one of the clearest and experimentally most accessible examples of the percolation problem. In a diluted magnet the infinite magnetic cluster present above the percolation limit is a self-similar fractal object.[3] That is, it looks the same at each of several different magnifications. Its realization in a magnetic system has the advantage that the multitude of macroscopic and microscopic experimental probes available in magnetism can be applied to study its properties. Thus, in the experiments to be described below, it could be shown that, close to the percolation limit, the infinite cluster has the topology of a one-dimensional chain.

In the case of mixtures of different magnetic atoms, on the other hand, one may study such problems as the random anisotropy magnet, the competing-anisotropy problem, or the random-exchange problem. All these problems are of current theoretical interest, whereas their experimental study has until now been severely hampered by the lack of suitable materials.

We mention finally the random-field problem, which was one of the main topics at the last International Conference on Magnetism (San Francisco, August, 1985). In this problem the response of an antiferromagnetic system with (magnetic or nonmagnetic) impurities to an applied magnetic field yields new critical phenomena of physical interest. Here again the present series of compounds offers enormous possibilities for experimental studies, an obvious advantage being the fact, already mentioned, that the antiferromagnetic exchange interactions are relatively weak ($|J/k_B| \simeq$ 0.1–1 K), so that small magnetic fields ($\simeq$0.01–1 tesla) may already produce the desired effects.

We hope to show in this review why and how this class of coordination compounds is of such potential value for the study of magnetic ordering phenomena of

a great diversity. In this sense we are convinced that our own investigations should be considered only as a preliminary survey, and that these materials (which are relatively easy to prepare) can be of value to other workers as well. Another aim of this review is to demonstrate that the field of coordination chemistry provides an extremely rich potential source for new and interesting materials for the solid state physicist in general. This is a field that is presently left almost unexplored in terms of physical investigations. Thus we hope that our work will inspire other physicists and chemists to join in the attempt to extend the domains of solid state physics and chemistry to this particular discipline. Clearly, it is precisely the formation of interdisciplinary research groups that can further our knowledge here most rapidly and effectively.

II. Synthesis, Crystallography, and Superexchange Paths

The synthesis of $[M(C_5H_5NO)_6]X_2$, where M is an iron-series ion and X may be perchlorate, nitrate, fluoborate, iodide, or bromate, is generally straightforward. The original method[4] was simply to mix a methanolic solution of the hydrated metal perchlorate with another of the ligand. The complex precipitates and it may be redissolved for slow crystal growth. Depending on the particular salt, a number of other organic solvents such as dimethylformamide (DMF) have been used for growing single crystals. Some caution is necessary here, for it has been claimed[5,6] that, at least with copper, some of the C_5H_5NO ligand is replaced in the lattice by molecules of the solvent.

The great interest for magnetic investigations of these materials can be attributed to the crystallographic simplicity of their structure observed, e.g., in the simultaneous X-ray investigations of $[Ni(C_5H_5NO)_6](BF_4)_2$,[7] $[Mn(C_5H_5NO)_6](ClO_4)_2$,[8] and $[Co(C_5H_5NO)_6](ClO_4)_2$.[9] It was discovered that these materials, which are all isomorphous, belong to the rhombohedral space group $R\bar{3}$ and have but one molecule in the unit cell. The high symmetry of the lattice of magnetic ions allows a comparison of the magnetic properties with theories for simple magnetic model systems, as have been extensively developed in the last 10 or 20 years within the theory of phase transitions and critical phenomena.[10]

There is now available crystallographic information on 18 salts of the formula $[M(C_5H_5NO)_6]X_2$ and these are listed in Table I. Some of the characterizations have been done by means of X-ray powder patterns, but at least 13 of the substances have been subjected to complete single-crystal structure analysis. There is agreement that every single example is isomorphous with all the others; many in fact are isostructural. This is rather remarkable when one considers the variety of both metal ion and counter ion. This is perhaps the largest series of isomorphous metal complexes extant.

A [001] projection of one layer of the unit cell of $[Co(C_5H_5NO)_6](ClO_4)_2$ is illustrated in Figure 1a. The crystallographically imposed S_6 point symmetry of the cation is obvious. Within experimental error, the CoO_6 grouping has been found to be perfectly octahedral at room temperature; this is true as well of all the other crystals investigated, even those of the Jahn–Teller ion, copper! The Co–O–N angle is about 120°, which allows

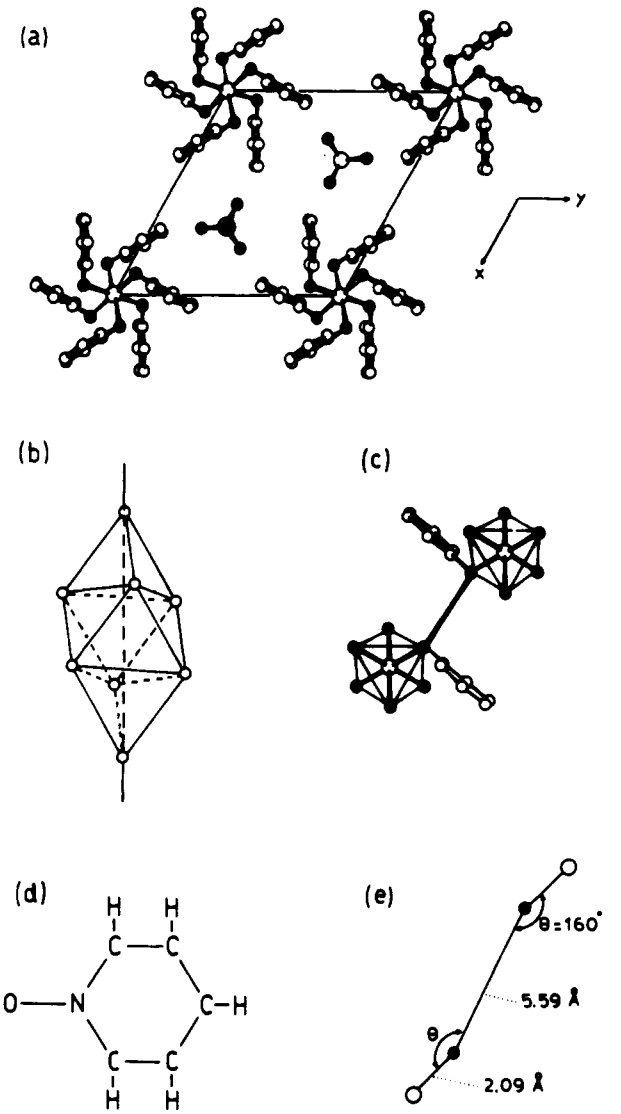

Figure 1. (a) A projection along the c axis of one layer of the hexagonal unit cell of $[Co(C_5H_5NO)_6](ClO_4)_2$. The Co^{2+} ions are on the corners (large open circles) and are octahedrally surrounded by the oxygens (filled circles) belonging to the NO groups (rings of small open circles). The ClO_4^- ions fill in the trigonal holes between the $[Co(C_5H_5NO)_6]^{2+}$ cations within each layer, and are composed of chlorine atoms (open circles) that are tetrahedrally surrounded by oxygen atoms (filled circles). It is noted that the Co^{2+} ions shown are next nearest magnetic neighbors to one another. (b) The rhombohedral cell formed by the Co^{2+} ions. (c) The superexchange path connecting Co^{2+} ions that are nearest magnetic neighbors. (d) Chemical structure of the C_5H_5NO ring. (e) Bond lengths and bond angles in the nearest-neighbor superexchange path shown in Figure 1c. Reproduced with permission from ref 20. Copyright 1976 Elsevier, Amsterdam.

the pyridine rings to bend out of the way and thereby provide an oxygen–oxygen superexchange path between adjoining metal ions. The perchlorate anions fill the trigonal holes between the cations.

The packing of the molecules in the lattice is intermediate between simple cubic (rhombohedral angle $\alpha = 90°$) and face-centered cubic ($\alpha = 60°$), since α is typically found as about 81°, a value quite close to that of the ideal simple cubic cell. The rhombohedral unit cell formed by the metal atoms is depicted in Figure 1b. With regard to the superexchange paths connecting the cobalt (or other metal) ions, as shown in Figure 1, parts c and d, a reference Co^{2+} ion is connected to its six nearest magnetic neighbors (at a distance of $\simeq$ 9.6 Å)

TABLE I. Rhombohedral Cell Constants of $[M(C_5H_5NO)_6]X_2$

compd	a, Å	α, deg	V, Å^3	ref
$[Mn(C_5H_5NO)_6](BF_4)_2$	9.72	81.3	888	11
$[Mn(C_5H_5NO)_6](ClO_4)_2$	9.69	81.1	870	11
	9.61	81.3		8
$[Fe(C_5H_5NO)_6](ClO_4)_2$	9.68	81.2	878	11
	9.640	81.06	866.3	12[a]
$[Co(C_5H_5NO)_6](BF_4)_2$	9.61	81.5	861	11
$[Co(C_5H_5NO)_6]ClO_4)_2$	9.63	81.2	864	11
	9.617	81.16		9[a]
	9.619	81.19	861.3	12[a]
$[Co(C_5H_5NO)_6](NO_3)_2$	9.49	83.3		13
	9.489	83.41	839	14[a]
$[Co(C_5H_5NO)_6]I_2$	9.563	82.46		15
$[Ni(C_5H_5NO)_6](BF_4)_2$	9.579	81.36	851.7	7, 11[a]
$[Ni(C_5H_5NO)_6](ClO_4)_2$	9.60	81.1	856	11
$[Ni(C_5H_5NO)_6](NO_3)_2$	9.486	83.26	837	16[a]
$[Ni(C_5H_5NO)_6](BrO_3)_2$	9.513	84.58	850	17[a]
$[Cu(C_5H_5NO)_6](BF_4)_2$	9.60	81.5	858	11
	9.621	81.46	864	18[a]
$[Cu(C_5H_5NO)_6](ClO_4)_2$	9.63	81.1	865	11
	9.620	81.21	862	18[a]
	9.605	81.10	857.1	12[a]
$[Cu(C_5H_5NO)_6](NO_3)_2$	9.504	83.41	843	14[a]
$[Zn(C_5H_5NO)_6](ClO_4)_2$	9.632	81.07	864	18[a]
$[Zn(C_5H_5NO)6](BF_4)_2$	9.621	81.25	862	18[a]
$[Mg(C_5H_5NO)_6](ClO_4)_2$	9.65	81.4	870	11
$[Hg(C_5H_5NO)_6](ClO_4)_2$	9.76	81.1	898	11

[a] Complete structure analysis.

by *equivalent* superexchange paths, consisting of a nearly collinear Co–O---O–Co bond, in which the Co–O and the O---O distances are about 2.1 and 5.6 Å, respectively. Since the pyridine rings are diverted away from this bond, one expects the superexchange to result from a direct overlap of the oxygen wave functions. From the fact that the superexchange pathway is nearly linear, the magnetic interactions can be expected to be antiferromagnetic,[19] as is indeed found in all the investigated compounds.

Next-nearest-neighbor (nnn) interactions are expected to be much less important,[20] since the nnn metal atoms are very much further apart and are connected by much less favorable exchange paths. Furthermore, due to the nearly cubic symmetry, the (long-range) dipolar interactions are negligible as compared to the magnetic exchange interactions, small as these may be. This has been confirmed by numerical calculations and experiment. Thus, since each metal ion is connected equivalently to its six nearest magnetic neighbors only, and in a lattice of nearly simple cubic symmetry, theoretical predictions based upon the simple cubic (s.c.) magnetic lattice should be applicable to a very high degree of approximation.

In this respect we may add that the perchlorate or other counter ions are found to have only a minor influence on the magnetic exchange interaction. This is to be expected since any such superexchange path would involve at least one additional oxygen atom from the perchlorate in addition to the two oxygens from C_5H_5NO groups.

III. Crystal-Field Effects and Paramagnetic Behavior

A decisive factor in determining the energy level structure of the electronic spins of the complexes with C_5H_5NO is the large crystal field or single-ion anisotropies which are encountered. This was recognized from magnetic data long before the crystal structure analyses were reported, and was at the time assumed to be due to gross geometric distortions. However the latter has not proved to be true (because of the perfectly octahedral geometry of the $[M(C_5H_5NO)_6]^{2+}$ cation), so that an explanation has to be sought elsewhere. A likely explanation involves the orientation of the C_5H_5N–O grouping relative to the threefold axis of the cation.[9] Thus, even though the octahedron around the metal ion formed by the oxygens of the ligands is perfectly cubic, the pyridine rings attached to the oxygen atoms render the symmetry of the molecule as a whole to be trigonal. From molecular orbital calculations,[21] it can be shown that this results in a trigonal component of the crystal field acting on the metal ions that may constitute a significant deviation from pure cubic symmetry.

TABLE II. Representative Single-Ion Magnetic Parameters

compd	$g_\parallel$	$g_\perp$	D/k_B, K	S	ref
$[Mn(C_5H_5NO)_6](ClO_4)_2$	2.002	2.002	0.054	5/2	8
$[Fe(C_5H_5NO)_6](ClO_4)_2$	9.0	0.6		1/2	22–25
$[Co(C_5H_5NO)_6](ClO_4)_2$	2.26	4.77		1/2	26
$[Co(C_5H_5NO)_6](NO_3)_2$	2.27	4.83		1/2	13
$[Ni(C_5H_5NO)_6](ClO_4)_2$	2.32	2.33	6.26	1	27
$[Ni(C_5H_5NO)_6](NO_3)_2$	2.25	2.29	5.69	1	16

A selection of data obtained for the single-ion anisotropies is listed in Table II; with the exception of the manganese data, all the results are derived from measurements at low temperatures and refer only to the isolated ground state of the system. These crystal-field anisotropies are quite large; for example, the zero-field splittings in the nickel salts, as given by the D/k_B values, are among the largest yet measured. The strong crystal-field effects are reflected, for the iron and cobalt salts, in the large anistropies in the g-values appropriate to the low-lying ground doublets, with effective spin $S = {}^1/_2$. As will be shown below, these crystal-field anisotropies play a decisive role in the type of magnetic ordering phenomena these systems undergo. Throughout this paper, "parallel" and "perpendicular" refer to orientations with respect to the c-axis of the rhombohedral unit cell.

Consider, for example, the Fe^{2+} ion in $[Fe(C_5H_5NO)_6](ClO_4)_2$.[22] In a cubic field the Fe^{2+} ion ($3d^6$; $L = 2$, $S = 2$) has the Γ_5 triplet as the lowest orbital level, which is split into a doublet and a singlet by a trigonal distortion. The crystal-field distortion is so large, as measured by Mössbauer spectroscopy,[23–25] that an isolated spin-orbit doublet is found as the ground state. The nearest level is at 170 K above the ground doublet. At temperatures relevant to the magnetic ordering (below 1 K) only the ground-state doublet will be appreciably populated, and we may treat this system within the effective spin $S = {}^1/_2$ formalism. The experimental g values are $g_\parallel \simeq 9.0$ and $g_\perp \simeq 0.5$. As will be explained in section IV, this large anisotropy makes the iron(II) compounds of the series excellent examples of the $S = {}^1/_2$, simple cubic Ising antiferromagnet.

The situation with nickel(II) is simpler. Octahedrally coordinated nickel ($3d^8$; $L = 3$, $S = 1$) always has the orbital singlet $^3A_2$ as the ground state, which is well-isolated (typically by at least 8000 cm^{-1}) from the nearest excited orbital level, and which has a 3-fold spin degeneracy. So, the magnetochemistry of nickel(II) is governed by the isolated $^3A_2$ state, which is described in terms of its $|m_s\rangle = |\pm 1\rangle$ and $|0\rangle$ components.

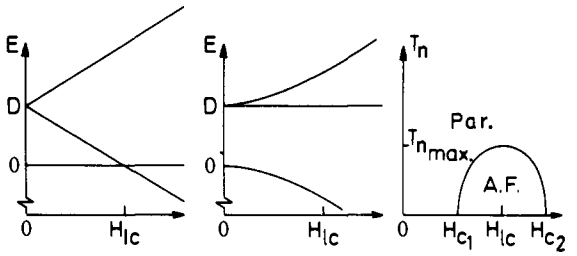

Figure 2. The lowest energy levels of Ni(II) in axial crystalline fields as a function of external magnetic field parallel (a) and perpendicular (b) to the principal molecular magnetic axes. (c) The hypothetical phase diagram for a system with large zero-field splitting.

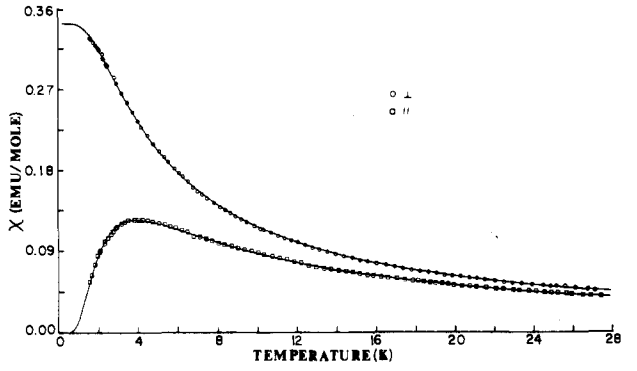

Figure 3. Isothermal susceptibilities of $[Ni(C_5H_5NO)_6](NO_3)_2$. Points are experimental (○ perpendicular; □ parallel) and fitted curves are described in the text. Reproduced with permission from ref 16. Copyright 1979 Physics Trust Publications.

The spin-Hamiltonian for trigonally distorted, six-coordinate nickel(II) may thus be written as ($S = 1$)

$$H = D[S_z^2 - (1/3)S(S+1)] + g\mu_B\vec{H}\cdot\vec{S} \qquad (1)$$

In zero external field, the first term in eq 1 causes the degenerate $m_s = \pm 1$ states to separate an amount D in energy from the nondegenerate $m_s = 0$ state. If the parameter D is positive the doublet level lies above the singlet, as illustrated in Figure 2. All of the $[Ni(C_5H_5NO)_6]X_2$ salts studied to date have a positive D/k_B, of magnitude 5 to 6 K. The quantity k_B is the Boltzmann constant, and μ_B is the Bohr magneton.

The energy levels and crystal field susceptibilities arising from Hamiltonian eq 1 may easily be calculated; the paramagnetic susceptibilities are found to be

$$\chi_\parallel = (2Ng_\parallel^2\mu_B^2/k_BT)\exp(-D/k_BT)\,x[1 + 2\exp(-D/k_BT)]^{-1} \qquad (2)$$

$$\chi_\perp = (2Ng_\perp^2\mu_B^2/D)[1 - \exp(-D/k_BT)]\,x[1 + 2\exp(-D/k_BT)]^{-1} \qquad (3)$$

where N is Avogadro's number.

A representative data set,[16] for $[Ni(C_5H_5NO)_6](NO_3)_2$, is illustrated in Figure 3. The parameters resulting from the analysis are $g_\parallel = 2.25 \pm 0.02$, $g_\perp = 2.29 \pm 0.02$, and $D/k_B = 5.69 \pm 0.05$ K. The g-values are typical, but the zero-field splitting (ZFS) is unusually large for nickel(II). The large ZFS explains why EPR has never been observed with these salts, even at 4.2 K. We note that in fitting the data in Figure 3, a correction has been applied for the presence of interactions between the magnetic ions.

As will be further discussed below, due to the large value of D/k_B, the magnetic exchange interactions (J)

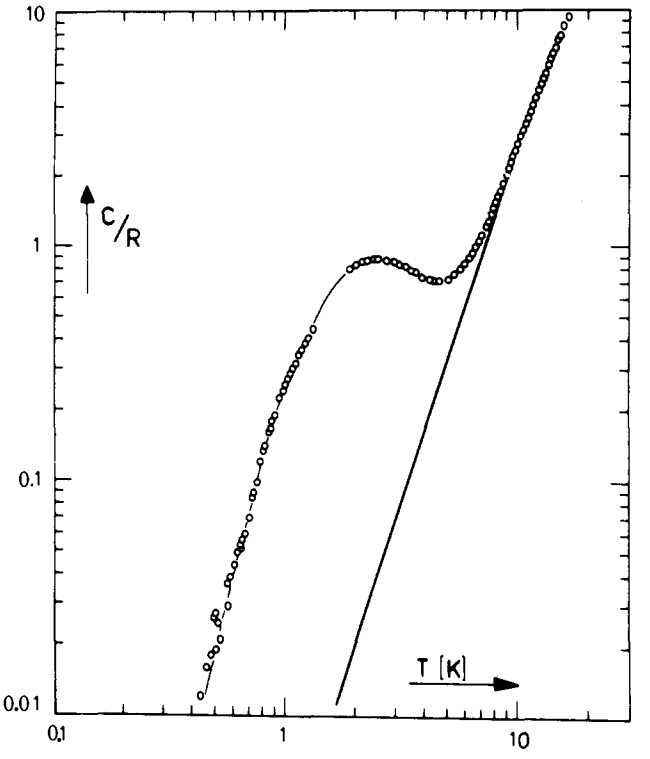

Figure 4. Zero-field specific heat data of $[Ni(C_5H_5NO)_6](ClO_4)_2$. Solid curves are for the Schottky and lattice contributions. Reproduced with permission from ref 28.

between the Ni^{2+} ions are *subcritical* in these materials, i.e., $|J| \ll D$ so that spontaneous magnetic ordering (in zero field) cannot occur for the simple reason that the upper doublet is already depopulated at temperatures $k_BT \simeq |J|$. In first approximation the presence of these exchange interactions may be accounted for within the molecular field formalism. The situation has been discussed in detail;[27] the exchange-corrected susceptibility χ' is given by

$$\chi_i' = \frac{\chi_i}{1 - (2zJ/Ng_i^2\mu_B^2)\chi_i} \qquad i = \parallel, \perp \qquad (4)$$

where χ_i are the crystal-field susceptibilities and $z = 6$ is the number of nearest magnetic neighbors. It is this molecular-field relationship that has been used to fit the data displayed in Figure 3. The exchange parameter zJ/k_B was found to be -1.5 ± 0.3 K. Similar results were obtained for the perchlorate,[27] while $[Ni(C_5H_5NO)_6](BrO_3)_2$ displays[17] crystal-field parameters that are quite similar but zJ/k_B is only -0.10 ± 0.05 K in this case.

The specific heat results confirm this analysis. The zero-field specific heat data[28] for $[Ni(C_5H_5NO)_6](ClO_4)_2$ are shown in Figure 4, along with a fitted curve calculated according to the sum of a Schottky term (C_s) and a lattice contribution (C_l). For $T < 10$ K the asymptotic Debye behavior for the phonon term is found as $C_l/Nk_B = aT^3$ with $a \simeq 2.5 \times 10^{-3}$ K^{-3}. Neglecting exchange, the Schottky term for the singlet-doublet system is given by

$$C_s/Nk_B = 2(D/k_BT)^2\exp(-D/k_BT)[1 + 2\exp(-D/k_BT)]^{-1} \qquad (5)$$

(for $D > 0$). From the fit the singlet-doublet separation is found as $D/k_B = 6.3 \pm 0.2$ K, in reasonable accord with the zero-field susceptibility analysis.

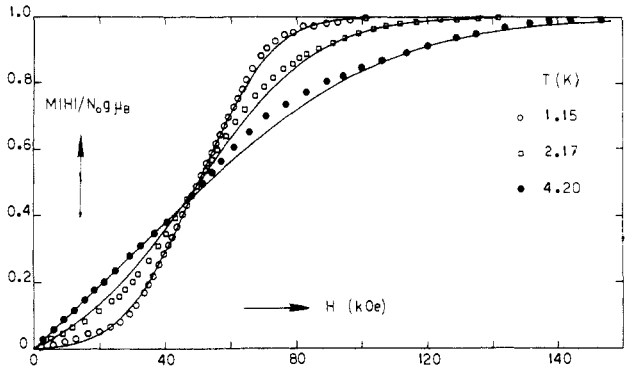

Figure 5. Magnetization curves of $[Ni(C_5H_5NO)_6](ClO_4)_2$. Solid curves give the calculated isothermal behavior. Reproduced with permission from ref 29. Copyright 1977 Elsevier, Amsterdam.

There is a highly interesting physical phenomenon associated with the fact that the crystallographic and magnetic structure of the $[Ni(C_5H_5NO)_6]X_2$ salts leads to subcritical exchange interactions zJ/k_B of the order of magnitude given above. Since all Ni^{2+} ions are equivalent in these rhombohedral crystals, the application of an external field of sufficient magnitude parallel to the symmetry (z) axis should produce a crossing of the singlet level by the lower doublet level, yielding in turn a magnetic ground state (see Figure 2). From $D/k_B \simeq 5$ K, one estimates this field to be $H_{lc} \simeq 50$ *kOe*. The magnetization data on $[Ni(C_5H_5NO)_6](ClO_4)_2$ (Figure 5) nicely confirm this picture.[29] Again, the data may be fitted with the singlet-doublet model with subcritical exchange interactions, yielding $g_\parallel = 2.32$, $D/k_B = 6.5 \pm 0.1$ K, and $zJ/k_B = -1.35 \pm 0.1$ K, consistent with the other determinations. We stress that this entire discussion concerns the paramagnetic behavior of the system. However, since for $H = H_{lc}$ the system has been brought into a magnetic ground state, it follows that the "subcritical" exchange interaction may then become effective and produce a magnetic ordering at sufficiently low temperatures. Indeed, such field-induced ordering phenomena have been observed in this material (at $T < 0.8$ K), as will be discussed in section VD. Also in the other Ni^{2+}–C_5H_5NO compounds, similar phenomena have been observed, as has recently been discussed elsewhere.[30]

Manganese(II) ($3d^5$; $L = 0$; $S = 5/2$) also exhibits a relatively large ZFS ($D/k_B \simeq 0.05$ K) in the $[Mn(C_5H_5NO)_6]X_2$ series. Some of the data are listed in Table II, and the results are best discussed in the section on magnetic ordering. The epr spectrum of manganese doped into the related molecule $[Zn(\gamma\text{-}CH_3\text{-}C_5H_4NO)_6](ClO_4)_2$ has also been reported.[31] The zero-field splitting parameter $D = 0.063$ cm^{-1}, and $\lambda = E/D = 0.06$, where E is the rhombic crystal-field term.

Let us turn next to the cobalt compounds, which also show highly interesting magnetic properties. For cobalt(II) ($3d^7$; $L = 3$; $S = 3/2$) in octahedral surroundings the ground state is the orbital triplet $^4T_1$, with 4-fold spin degeneracy. The spin-orbit coupling constant is large, $\lambda = -180$ cm^{-1} in the free ion, and so the resolution of the degeneracy of the ground state into six widely spaced Kramers doublets by the combined effects of spin-orbit coupling and an axial crystal-field term is an important feature of the electronic structure of this ion. One and the same doublet remains lowest in energy, regardless of the sign and magnitude of the axial crystal-field term, the nearest excited level being at least 100 cm^{-1} higher in energy. At temperatures at which only the ground level is appreciably populated ($T < 50$ K) this system may be described by an effective spin $S = {}^1/_2$. The orbital contribution of the nearby components of the $^4T_1(F)$ state causes the ground doublet in the weak cubic field limit to have an isotropic $g = 4.333$ but large anisotropy in the g values is expected as the crystal field becomes of symmetry lower than cubic. The three orthogonal g values are then expected to sum in first order to the value of 13. Depending on the sign of the axial distortion one can have either $g_\parallel \gg g_\perp$ or $g_\perp \gg g_\parallel$.

TABLE III. Experimental Parameters for $[Co(C_5H_5NO)_6](ClO_4)_2$[a]

(a) From EPR
$g_\parallel = 2.26 \pm 0.01$
$g_\perp = 4.77 \pm 0.01$
$A = (1.86 \pm 0.01) \times 10^{-3}$ cm^{-1}
$B = (3.84 \pm 0.01) \times 10^{-3}$ cm^{-1}

(b) From Susceptibility
$g_\parallel = 2.49 \pm 0.05$
$g_\perp = 4.70 \pm 0.05$
$\theta_\parallel = -0.28 \pm 0.05$ K
$\theta_\perp = -0.52 \pm 0.05$ K
$TIP_\parallel = (1.1 \pm 0.7) \times 10^{-3}$ emu mol^{-1}
$TIP_\perp = (2.4 \pm 0.7) \times 10^{-3}$ emu mol^{-1}

[a] Reproduced with permission from ref 26. Copyright 1976, American Chemical Society. A and B are the nuclear hyperfine splitting parameters, the θ's are the Weiss constants, and TIP is temperature-independent paramagnetism. For $[Co(C_5H_5NO)_6](NO_3)_2$, the susceptibility parameters are, from ref 13, $g_\parallel = 2.27 \pm 0.05$, $g = 4.83 \pm 0.05$, $\theta_\parallel = 0.0 \pm 0.05$ K, $\theta_\perp = -0.61 \pm 0.05$ K, TIP(∥) = 0.006 emu/mol and TIP(⊥) = 0.037 emu/mol.

For Co^{2+} doped into $[Zn(C_5H_5NO)_6](ClO_4)_2$, $g_\parallel = 2.26 \pm 0.01$ and $g_\perp = 4.77 \pm 0.01$ have been reported;[26] see Table III. The energy difference between the ground state doublet and the next higher doublet was estimated to be of the same order as λ, so that it will amount to about 200 K. This warrants the applicability of the $S = {}^1/_2$ formalism to the magnetic behavior of the $[Co(C_5H_5NO)_6]X_2$ compounds in the liquid ^{4}He temperature range, as will be explained below.

The fairly uncommon anisotropy observed in the g-values, namely $g_\perp \gg g_\parallel$, has important implications for the magnetic ordering phenomena displayed by these compounds.[20] As explained below, for such a kind of anisotropy the magnetic interaction approximates that considered in the XY model of magnetism. In fact, these materials were the first examples discovered of the simple cubic, XY model of magnetism.

The general subject of zero-field splittings and the ways that they control magnetic ordering phenomena have recently been reviewed.[30]

Finally, the last ion to be discussed here is copper(II) ($3d^9$; $L = 2$, $S = {}^1/_2$), which is a well-known Jahn–Teller ion. In this respect it is surprising that the $[Cu(C_5H_5NO)_6]X_2$ salts are isomorphous with those of the other metal ions, and that the $[Cu(C_5H_5NO)_6]^{2+}$ ion is only slightly distorted from regular octahedral symmetry. However, this is based on crystallographic measurements at room temperature; at lower temperatures, Jahn–Teller distortions do set in, as will be discussed in section VE.

At room temperature, the copper ions behave in the usual fashion as paramagnetic $S = {}^1/_2$ ions with g slightly greater than 2. A selection of EPR data is presented in Table IV. Differences among the spectra

TABLE IV. Summary of ESR Data for $[Cu(C_5H_5NO)_6]X_2$

ref	compd	g_x	g_y	g_z
O'Connor[28]	Cu^{2+}: $ZnL_6(ClO_4)_2$	$g_\perp$ = 2.17 (2)		$g_\parallel$ = 2.20 (2)
Wood[32]	Cu^{2+}: $ZnL_6(ClO_4)_2$	2.092	2.099	2.392

have been discussed;[32,33] in certain cases, solvent may be included in the coordination sphere.[5,6]

IV. Magnetic Models[1,30,34-38]

As already mentioned above, the pyridine *N*-oxide compounds are rather unique in that they provide a series of excellent examples of magnetic model systems that had previously not been studied experimentally. In order to illustrate this, we must first present a brief overview of magnetic model systems, since this is indispensable for an understanding of what follows.

Magnetic model systems can be divided according to the type of interaction between the magnetic moments, the lattice formed by the moments, the value of the spin, and so on. The interactions may be long-range as for the dipolar interaction (which falls off as r^{-3}), or short-range, as for the superexchange interaction which depends exponentially on the mutual separation of the ions. The magnetic lattice formed by the moments may be 1-, 2-, or 3-dimensional (chains, layers or cubic). In practice, 1- or 2-D lattices may be approximated in compounds where the exchange is very weak in 2 or 1 spatial directions, for instance when the magnetic ions are much farther apart along those directions. Furthermore, the interaction between nearest magnetic neighbors (on an arbitrary lattice) can be isotropic or anisotropic. In the simplest case we may describe the anisotropic interactions between nearest-neighbor ions i and j by means of the uniaxially symmetric Hamiltonian

$$H = -2\sum_{i,j}\{J_{xy}(S_{ix}S_{jx} + S_{iy}S_{jy}) + J_zS_{iz}S_{jz}\} \qquad (6)$$

where the limiting cases $J_{xy} = J_z$, $J_z = 0$, and $J_{xy} = 0$ correspond with the Heisenberg, XY, and Ising models, respectively. In practice, for 3*d* metal compounds an anisotropy in the interaction arises in most cases from crystal field effects through the spin-orbit coupling. Consequently, ions with zero (Mn^{2+}) or quenched orbital moments (Ni^{2+}, Cu^{2+}) are often good approximations of the Heisenberg model, whereas Fe^{2+} and Co^{2+} compounds may provide examples of either the Ising or the XY models, depending on the sign and type of the deviations from cubic crystal field anisotropy of the metal ion.

In this respect it is of interest to mention that our studies of the magnetic ordering phenomena in the C_5H_5NO compounds were started more than a decade ago with the aim of finding experimental approximations of the XY model for which no good examples were known at the time. From EPR studies, the anisotropy in the *g*-tensor for the lowest Kramers doublet in the $[Co(C_5H_5NO)_6]^{2+}$ salts had been determined, and pointed to the result that $g_{xy} \gg g_z$. Since it can easily be shown that the anisotropy in the interaction between the effective spins $S = {}^1/_2$ for the doublet will be given by $J_{xy}/J_z \simeq (g_{xy}/g_z)^2$, it seemed worthwhile to look for magnetic ordering at low temperatures in these materials. At the time it was by no means certain whether the exchange interaction in such a dilute lattice would be sufficiently strong to yield magnetic ordering phenomena in the (reasonably) accessible temperature range $T > 0.1$ K.

TABLE V. Transition Temperatures T_c and Antiferromagnetic Exchange Constants J/k_B of the Compounds Which Have Been Found To Become Magnetically Ordered

compd	$-J/k_B$, K	T_c, K	ref
$[Mn(C_5H_5NO)_6](BF_4)_2$	0.006	0.158	39
$[Fe(C_5H_5NO)_6](ClO_4)_2$	0.32	0.719	22
$[Co(C_5H_5NO)_6](ClO_4)_2$	0.20	0.428	20
$[Co(C_5H_5NO)_6](BF_4)_2$	0.174	0.357	20
$[Co(C_5H_5NO)_6](NO_3)_2$	0.220	0.458	15
$[Co(C_5H_5NO)_6]I_2$	0.243	0.500	15
$[Ni(C_5H_5NO)_6](ClO_4)_2$	0.2	0.75[a]	40, 41
$[Ni(C_5H_5NO)_6](NO_3)_2$	0.2	0.89[b]	42
$[Cu(C_5H_5NO)_6](ClO_4)_2$	1.02[c]	0.142	33
$[Cu(C_5H_5NO)_6](BF_4)_2$	1.10[d]	0.62	33

[a] In an applied field of 48 kOe. [b] In an applied field of 42 kOe. [c] Linear-chain value; see section VE. [d] Quadratic plane value; see section VE.

The observed values for the magnetic transition temperatures and exchange constants are compiled in Table V. Indeed, the cobalt salts proved to be excellent examples of the $S = {}^1/_2$, XY antiferromagnet. Furthermore, it can be shown that the same crystal field symmetry that leads to g_{xy} being much larger than g_z for the cobalt ion will leave a low-lying Ising doublet with $g_\parallel \gg g_\perp$ as the ground state for Fe^{2+}. Accordingly, the Fe^{2+} compound shows a magnetic behavior well-described by the s.c. Ising, $S = {}^1/_2$ model. As already mentioned, for Ni^{2+} the same crystal-field symmetry splits the $S = 1$ triplet state into a lower orbital singlet and an upper doublet. In the $[Ni(C_5H_5NO)_6]^{2+}$ salts the singlet–doublet splitting is large compared to the exchange, so that magnetic ordering can only occur in an applied field sufficiently strong to produce a (near) crossing of a doublet level with the ground singlet. Prior to our work, field-induced magnetic ordering phenomena in such a singlet-ground-state system had not been studied experimentally due to the lack of suitable materials. So also in this case the pyridine *N*-oxide compounds have provided a first example.

Lastly, the Cu–C_5H_5NO compounds were found to show low-dimensional magnetic behavior. The perchlorate salt was found to behave as an antiferromagnetic $S = {}^1/_2$ Heisenberg chain, whereas the fluoborate salt proved to be the first example of an antiferromagnetic Heisenberg quadratic layer with a spin value as low as $S = {}^1/_2$. In these compounds the low-dimensional properties are found to be due to a lack of overlap of the Cu^{2+} d orbitals in 1 or 2 crystallographic directions. This is a consequence of the cooperative Jahn–Teller ordering of the octahedra around the copper ions, which ordering is ferro- and antiferrodistortive, respectively, for $[Cu(C_5H_5NO)_6](BF_4)_2$ and $[Cu(C_5H_5NO)_6](ClO_4)_2$. A similar antiferro-distortive ordering of the fluorine octahedra has been shown in fact to produce 1-d antiferromagnetic behavior in $KCuF_3$, which belongs to the series of cubic perovskite compounds AMF_3.

Thus, the magnetic investigations of these materials have revealed a variety of quite interesting and often new phenomena, which we shall now separately discuss more extensively.

TABLER VI. Critical Thermodynamic Parameters for the $S = {}^1/_2$ s.c. Magnetic Models Compared with the Experimental Values. The quantities S_∞ and S_c Correspond to the Entropy at $T = \infty$ and $T = T_c$, Respectively, Whereas E_0 and E_c Denote the Magnetic Energy at $T = 0$ and at $T = T_c$

	$k_BT_c/\|J\|$	S_c/R	$(S_\infty - S_c)/R$	$-E_c/RT_c$	$-E_0/RT_c$
Heisenberg (ferromagnetic)	1.68	0.43	0.26	0.60	0.89
XY	2.02 (2)	0.44 (2)	0.25 (1)	0.45 (1)	0.78
Ising	2.255	0.558	0.135	0.220	0.665
$[Co(C_5H_5NO)_6](BF_4)_2$	1.98 (4)	0.45 (2)	0.25 (1)	0.47 (2)	0.81 (3)
$[Co(C_5H_5NO)_6](ClO_4)_2$	2.02 (4)	0.47 (2)	0.24 (1)	0.43 (2)	0.79 (3)
$[Co(C_5H_5NO)_6](NO_3)_2$		0.44 (2)	0.25 (1)	0.45	
$[Co(C_5H_5NO)_6]I_2$		0.42 (2)	0.26 (1)	0.47	
$[Fe(C_5H_5NO)_6](ClO_4)_2$		0.55	0.19	0.335	0.434

V. Magnetic Ordering

The $[M(C_5H_5NO)_6]X_2$ compounds known to date which undergo magnetic ordering in one fashion or another are listed in Table V. This table must be used judiciously because it is the different ways in which these materials order which is of so much interest.

A particular advantage in studying these systems is that the magnetic ordering generally occurs below 1 K. Thus, specific heat studies could be advantageously exploited[43] in elucidating many of these phenomena, because the lattice contribution is so small (cf. Figures 4 and 24). For temperatures below 10 K, the phonon specific heat has been found to be well-approximated by the term $C_{lat}/Nk_B = aT^3$, with a $\simeq 2.5 \times 10^{-3}$ K^{-3} for all of the compounds. Thus, the data measured below 1 K can be ascribed to the magnetic specific heat. (At very low temperatures, additional small nuclear hyperfine contributions have been observed with several of the compounds.)

We now discuss each of these systems in turn, according to the metal ion.

A. Manganese(II)

Magnetic ordering occurs at 0.158 K in $[Mn(C_5H_5NO)_6](BF_4)_2$, the only manganese salt in this series yet examined at low temperatures.[39] The analysis of the specific heat in terms of a magnetic model system is difficult, because the exchange interaction, zero-field splitting and nuclear hyperfine coupling are all comparable in magnitude. The relatively large ZFS of 410 Oe (54 mK) is evident in the EPR spectrum.[8] It has been estimated that the total splitting of the ^6S ground-state electronic and nuclear levels caused by the combined action of crystal-field and hyperfine interaction is into a ladder of 17 (degenerate) states, with a total splitting of the order of 463 mK. Since $T_c = 158$ mK is only a third of this, the higher lying energy levels will already be partly depopulated at the temperature of magnetic ordering and the effective value of the electronic spin will be varying with temperature, decreasing from $S = {}^5/_2$ for $T \gg T_c$ to some lower value in the ordered region. The exchange constant, J/k_B, has been estimated as about -6 mK. No other measurements have yet been reported on this material.

B. Iron(II)

The magnetic energy level scheme of $[Fe(C_5H_5NO)_6](ClO_4)_2$ was first deduced by Sams and Tsin[23-25] from Mössbauer data on polycrystalline samples, which suggested that the magnetic properties should be describable in terms of an effective-spin $S = {}^1/_2$ ground-state doublet, with the highly anisotropic splitting

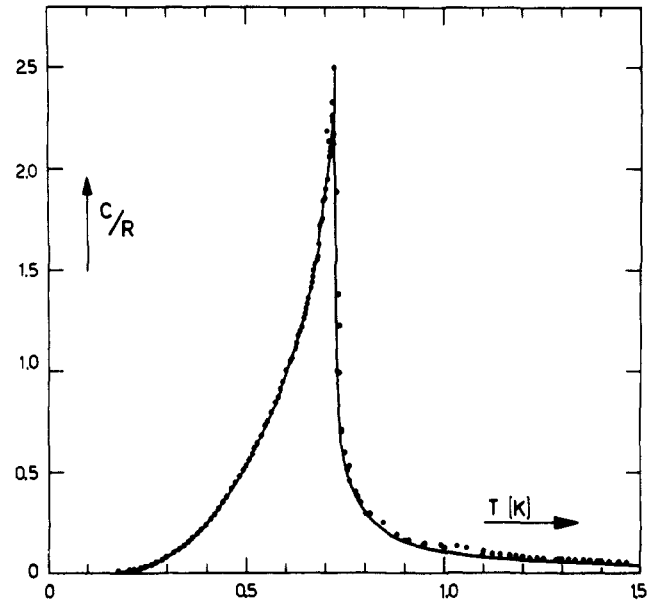

Figure 6. The magnetic specific heat of $[Fe(C_5H_5NO)_6](ClO_4)_2$. Reproduced with permission from ref 22. Copyright 1978 Elsevier, Amsterdam.

factors $g_\perp = 9.0$ and $g_\perp \simeq 0.6$. The Mössbauer results for the g tensor give a powder value $\langle g \rangle = 5.2 \pm 0.6$. The next higher lying energy levels were estimated to be at least 170 K above the ground state doublet, so that they will not be appreciably populated at temperatures below 4.2 K. As a consequence, the Ising Hamiltonian $H = -2J\sum_{i,j}S_{iz}S_{jz}$ should be closely approximated in this compound.

The specific heat of $[Fe(C_5H_5NO)_6](ClO_4)_2$ is displayed in Figure 6, after subtraction of the small lattice contribution.[22] The magnetic specific heat is seen to feature a sharp anomaly at $T_c = 0.719 \pm 0.003$ K. The points are experimental, while the solid curves in the plot represent the prediction for the specific heat of the simple cubic (s.c.), $S = {}^1/_2$ Ising model obtained from high- and low-temperature series expansions of the free energy. The fit of the theory of the experiment yields the value $|J/k_B| = 0.32 \pm 0.01$ K for the exchange constant. In Table VI we compare the critical energy and entropy parameters found from the data with the s.c. Ising predictions. The agreement below T_c is excellent, whereas above T_c the experimental values are somewhat in excess. This may be attributed to a small amount of Fe^{3+} contamination, which is very difficult to avoid in the sample preparation.

The susceptibility of polycrystalline $[Fe(C_5H_5NO)_6](ClO_4)_2$ is displayed in Figure 7. The experiments[44] were made on powdered samples, since the growth of single crystals proved to be very difficult. Nevertheless, the powder data are representative for the parallel an-

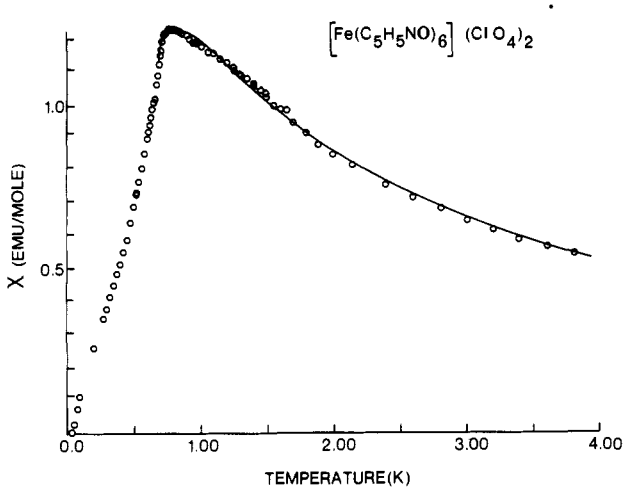

Figure 7. Susceptibility of polycrystalline $[Fe(C_5H_5NO)_6](ClO_4)_2$. The points are experimental, while the curve is the fit described in the text. Reproduced with permission from ref 44. Copyright 1980 American Institute of Physics.

tiferromagnetic susceptibility, because of the extreme anisotropy in the expectation values for the ground doublet. Since the contributions of $\chi_\perp$ and $\chi_\parallel$ to the powder susceptibility $\chi_p = (\chi_\parallel + 2\chi_\perp)/3$ have to be scaled by their respective g values squared, the fact that $g_\perp/g_\parallel \leq 0.1$ implies that $\chi_\perp$ will only contribute at most a few percent to χ_p.

The ordering temperature obtained from the point of maximum slope in the χ-vs.-T curve is 700 ± 10 mK, which agrees well with the result obtained from the specific-heat measurements. The data above 720 mK were fitted using calculations for the parallel susceptibility of the S = $^1/_2$, simple-cubic Ising antiferromagnet,[44] as illustrated in Figure 7. The resulting parameters are $\langle g \rangle = 5.38 \pm 0.05$ and $J/k_B = -0.34 \pm 0.02$ K. The agreement with the above mentioned values is excellent. For the Ising model on loose-packed lattices, the sign of the exchange is irrelevant for the specific heat, so that the sign of the exchange constant cannot be determined from specific-heat measurements. Therefore, it is the susceptibility data that confirm the antiferromagnetic sign of the interaction between the nearest magnetic neighbors. One may conclude that $[Fe(C_5H_5NO)_6](ClO_4)_2$ provides an excellent example of the simple cubic, $S = {}^1/_2$ Ising antiferromagnet.

C. Cobalt(II)

1. $[Co(C_5H_5NO)_6](ClO_4)_2$ and Related Compounds

The first experimental examples of the three-dimensional XY model were provided by the specific heat measurements on $[Co(C_5H_5NO)_6](ClO_4)_2$ and $[Co(C_5H_5NO)_6](BF_4)_2$.[20] Subsequently, the specific heats of $[Co(C_5H_5NO)_6](NO_3)_2$ and $[Co(C_5H_5NO)_6]I_2$ were shown to follow the predictions of this model as well.[15] That all these systems should behave similarly is due to their crystallographic and magnetic isomorphism.

The specific heat results are shown in Figure 8. Transitions to long-range magnetic order are observed at $T_c = 0.428$ (3) K and $T_c = 0.357$ (3) K for the perchlorate and the fluoborate compounds, respectively. The small difference in the values of T_c confirms the assumption that possible superexchange paths via the ClO_4^- and BF_4^- anions are relatively unimportant contributors to the net magnetic interaction.

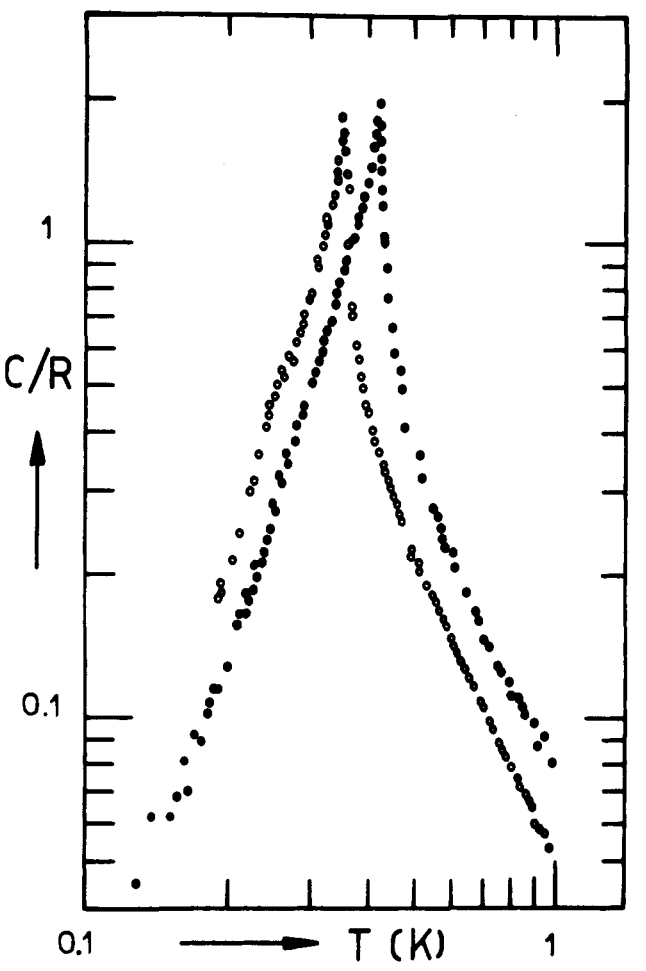

Figure 8. Experimental specific-heat data for $[Co(C_5H_5NO)_6](BF_4)_2$ (open circles), and $[Co(C_5H_5NO)_6](ClO_4)_2$ (filled circles). Since no evidence for lattice or hyperfine contributions to the specific heat is observed, the data can be regarded as representing the magnetic specific heat. Reproduced with permission from ref 20. Copyright 1976 Elsevier, Amsterdam.

The reason for extending these studies to a total of four salts was threefold: (i) to evidence the similarity in the magnetic behavior, (ii) to study the effect of the type of X^- anion on the magnetic interactions, and (iii) by changing to the smaller I^- and, in particular, NO_3^- anions it was hoped to obtain a compound with a higher T_c, which would enable a more extensive study of the specific heat in the low-temperature spin-wave region.

The expected similarity in the magnetic behavior of the compounds is confirmed by the striking resemblance of the two curves in Figure 8, which suggests that they can be brought into a near coincidence when a relative temperature scale, such as T/T_c or k_BT/J, is used. This is demonstrated in Figure 9 in which it is seen that in fact a collection of data on two compounds of the series fall on one and the same curve. Here we have plotted the specific heats as a function of $k_BT/|J|$, the exchange constants having been determined by fitting the data to the available predictions for the s.c. XY model with $S = {}^1/_2$, which are the solid curves in this figure. For $T > T_c$ the prediction is based on high-temperature series expansions of the free energy of this model. This fits the data to within 1–2% of T_c. At low temperatures, there is a spin-wave theoretical prediction for this model, drawn up to $k_BT/|J| \simeq 1$, above which this low-temperature theory will lose its validity. We note that spin-wave theory predicts a T^3

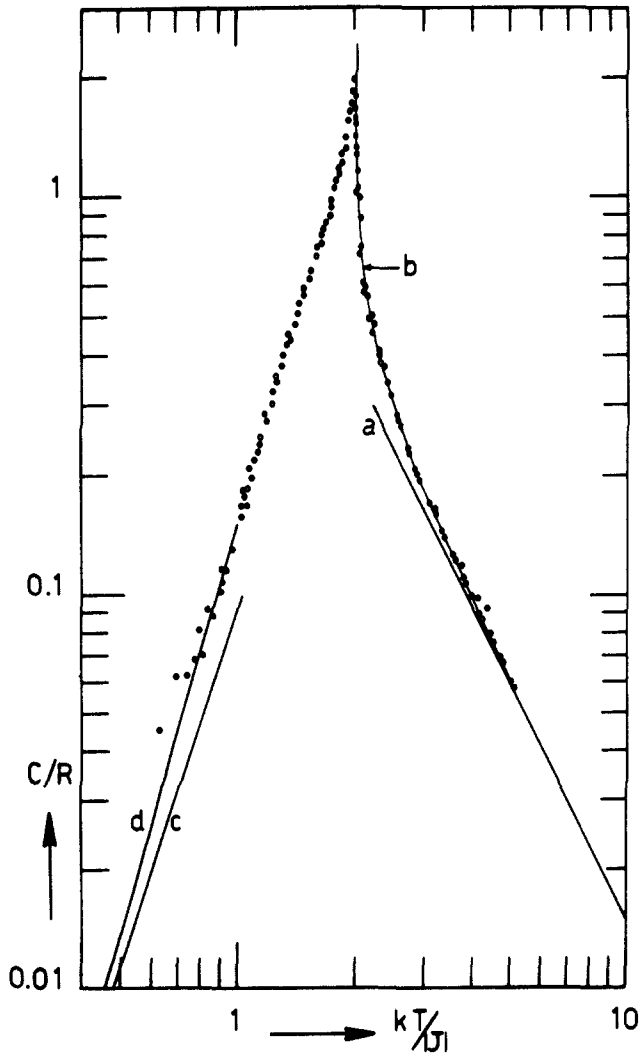

Figure 9. The specific-heat data from two cobalt salts plotted vs. the relative temperature k_BT/J. Curves a–d are theoretical predictions for the s.c. XY model with $S = {}^1/_2$.

behavior in the limit $T \rightarrow 0$ for the specific heat of the 3-D, XY model, which seems to be obeyed by these compounds.

One may conclude from this figure and from the data in Table VI that the experimental results are in excellent agreement with the XY model predictions, in particular when compared with the theoretical values for the s.c. Heisenberg and Ising models. The theoretical results for the XY model are seen to be intermediate between those for the Heisenberg and Ising models.

An estimate of the amount of anisotropy in the compounds may be deduced from the measured g values. In section III, we found $g_\parallel = 2.26$ (1) and $g_\perp = 4.77$ (1) from EPR measurements on cobalt(II) doped into $[Zn(C_5H_5NO)_6](ClO_4)_2$, and $g_\parallel = 2.49$ (5) and $g_\perp = 4.70$ (5) from susceptibility measurements on the pure cobalt compound ($1.5 < T < 20$ K). As discussed above, a ratio $J_{xy}/J_z \simeq 3.2$ is then obtained (eq 6), pointing to a strong XY-type anisotropy in the effective interaction.

Similar studies were reported on $[Co(C_5H_5NO)_6](NO_3)_2$ and $[Co(C_5H_5NO)_6]I_2$.[15] In fact, the anisotropy in the g-tensor is quite similar for all the cobalt compounds, and so one anticipates the same effective anisotropy in the exchange. Such a large planar-type spin anisotropy is apparently sufficient to yield a thermo-

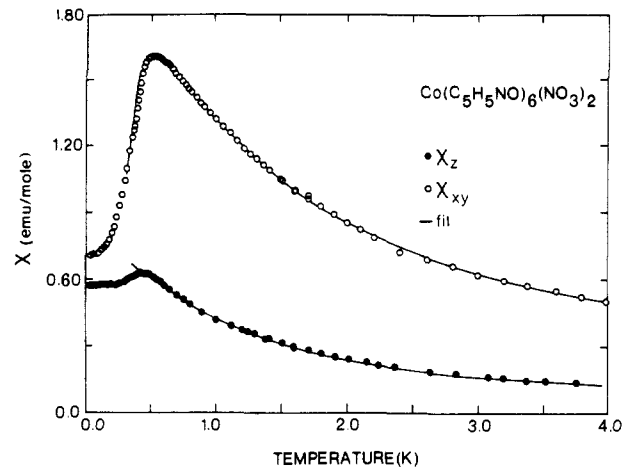

Figure 10. Measured susceptibilities (points) of $[Co(C_5H_5NO)_6](NO_3)_2$ and the fits as described in the text. The solid points refer to data parallel to the z axis, the open points to data perpendicular to the z axis. Reproduced with permission from ref 45. Copyright 1981 American Institute of Physics.

dynamic behavior corresponding quite closely to that of the pure XY model ($J_z = 0$). Indeed, the influence of the anisotropy on the thermodynamic behavior was studied, that is the variation with the parameter J_z/J_{xy}. It was found that the data may be equally well fitted by the theory for $J_z/J_{xy} \simeq 0.3$ as for $J_z = 0$, for the simple reason that in this range of values the thermodynamic quantities are fairly insensitive to variation of this anisotropy parameter.[15]

Susceptibility measurements[45] are in agreement with the specific heat results, and, in particular, show that the phase transition is indeed an antiferromagnetic one. This is of some importance, since here again the sign of J cannot be deduced from the specific-heat experiments. This is because, also for the XY model on loose-packed lattices the sign of the exchange constant is irrelevant for the specific heat.

The susceptibility data for $[Co(C_5H_5NO)_6](NO_3)_2$ below 4 K are illustrated in Figure 10. The data for χ_z and χ_{xy} show that the easy (xy) plane for the magnetic moments is perpendicular to the trigonal axis ($\chi_z \ll \chi_{xy}$), in agreement with the observed g anisotropy. A maximum in χ_{xy} occurs at 0.51 K. At lower temperatures the susceptibility drops and the value for T_c, as defined by the maximum in $\partial\chi_{xy}/\partial T$, is obtained as 0.432 ± 0.005 K. This is in reasonable agreement with the value found from the specific heat.

The solid curves in Figure 10 are fits to high-temperature series expansions[45] which yielded (with $J_z/J_{xy} = 0.31$) the parameters $J_{xy}/k_B = -0.219$ K, $g_{xy} = 4.99$ (5) and $g_z = 2.42$ (5). The behavior of the susceptibility below T_c is explained in ref 45.

2. Magnetic Ordering in $[Co(\gamma\text{-}CH_3\text{-}C_5H_4NO)_6](ClO_4)_2$

The hydrogen atoms in the pyridine N-oxide ring can be replaced by other groups, and thus γ-picoline N-oxide has been investigated as a ligand. This molecule, $\gamma\text{-}CH_3\text{-}C_5H_4NO$, contains a methyl group in the para position of the ring which significantly increases the size of the ligand molecule and changes the crystal structure of the compound substantially from that of the pyridine N-oxide complexes. The preparation of the samples is similar. The magnetic properties of $[Co(\gamma\text{-}CH_3\text{-}C_5H_4NO)_6](ClO_4)_2$ are appreciably different from

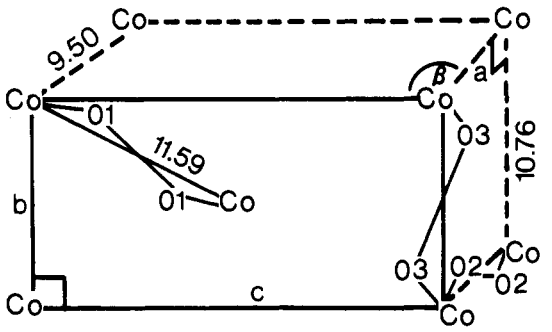

Figure 11. The possible superexchange paths in $[Co(\gamma\text{-}CH_3\text{-}C_5H_4NO)_6](ClO_4)_2$. Reproduced with permission from ref 46. Copyright 1981 Elsevier, Amsterdam.

those of $[Co(C_5H_5NO)_6](ClO_4)_2$. The cobalt salt is found to be isomorphous with the analogous copper and zinc salts of γ-picoline *N*-oxide.[46]

The material belongs to the space group $P2_1/c$ with two molecules in the monoclinic unit cell. The change of ligand leads to substantial distortions of the oxygen octahedra surrounding the Co^{2+} cations. The Co–O distances evidence local orthorhombic symmetry around the Co^{2+} ion (2.053, 2.109, and 2.128 Å). The most significant difference, however, is found in the crystal packing of the $[Co(\gamma\text{-picoline } N\text{-oxide})_6]^{2+}$ units into a largely two-dimensional network.[46] The lowering of the symmetry of the lattice also leads to an inequivalency of the superexchange paths connecting the Co^{2+} magnetic moments along the various crystallographic directions.

Since a nearly collinear Co–O---O–Co superexchange path is most important in the $[Co(C_5H_5NO)_6]X_2$ series of compounds, a comparable superexchange path in the crystal structure of $[Co(\gamma\text{-}CH_3\text{-}C_5H_4NO)_6](ClO_4)_2$ was sought. As was found with the pyridine *N*-oxide ligands, the picoline rings are diverted away from the Co–O---O–Co bond, which allows superexchange to result from a direct overlap of the oxygen wave functions. Examination of the structure (Figure 11) shows the following: along the *a* axis, there is such a Co–O---O–Co fragment, with Co–O(2) length of 2.128 Å, O(2)–O(2) distance of 5.442 Å, and Co–O(2)–O(2) angle of 157.7°. Along the *b* axis, another such fragment is found with Co–O(3) of 2.053 Å, O(3)–O(3) of 6.964 Å, and Co–O(3)–O(3) angle of 152°. Finally, in the *bc* plane there is a superexchange path between the cobalt atom at the origin of the unit cell and the one in the center of the *bc* rectangle. The Co–O(1) length is 2.109 Å, the O(1)–O(1) distance is 8.243 Å and the Co–O(1)–O(1) angle is 125.0°. The much larger O---O distance makes this path considerably less effective than those along *a* or *b*. In contrast, therefore, with the situation in $[Co(C_5H_5NO)_6](ClO_4)_2$, the Co atoms are not connected by equivalent superexchange paths in the various crystallographic directions.

The susceptibility results are illustrated in Figure 12 for three mutually perpendicular orientations of the crystal and clearly give evidence of antiferromagnetic ordering.[47] The easy axis was determined experimentally and was found to lie in the *ac* plane, 26° away from the *c* axis. This axis will be referred to as the *c'* axis. The other two orientations are along the *a'* axis, which is within the *ac* plane but perpendicular to the *c'* axis, and along the *b* axis. The critical temperature as defined by the maximum in $\partial\chi_{c'}/\partial T$, occurs at $T_c = 0.49(2)$ K. The parallel susceptibility $\chi_{c'}$ drops to a value which for the lowest temperatures approaches zero within the experimental accuracy. The susceptibilities measured along *a'* and *b* show the behavior expected for the perpendicular susceptibility of a (strongly anisotropic) antiferromagnet. At $T = 4.2$ K the measured susceptibilities point to an anisotropy in the *g* tensor of the order of $g_{c'}:g_b:g_{a'} = 1:0.79:0.59$. These splitting factors refer to the effective spin $S = {}^1/_2$ (Kramers) doublet expected for Co^{2+} in octahedral surrounding. The *g*-ratios imply that the nearest neighbor exchange interaction within the effective spin ${}^1/_2$ formalism will be quite anisotropic, since $J_{c'}:J_b:J_{a'} = g_{c'}{}^2:g_b{}^2:g_{a'}{}^2 = 1:0.63:0.35$. The magnetic behavior, therefore, should approach that of the Ising model ($J_b = J_{a'} = 0$), although basically the anisotropy is orthorhombic.

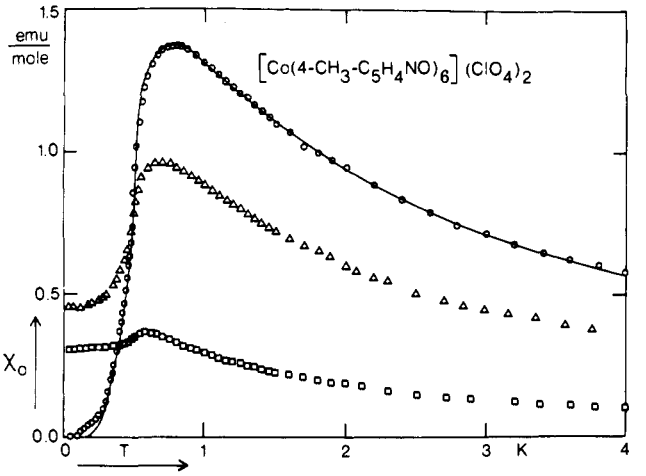

Figure 12. The susceptibilities along three orthogonal axes. The curve drawn through the *c'* axis data (circles) is the fit to the two-dimensional (quadratic) Ising model with $g_{c'} = 5.48$ and $J/k_B = -0.44$ K. Reproduced with permission from ref 47. Copyright 1981 Elsevier, Amsterdam.

The solid curve drawn in Figure 12 is a theoretical curve for a 2-D quadratic Ising lattice. A good fit over the entire measured temperature region was obtained using the set of parameters $g_{c'} = 5.48 \pm 0.10$ and $J/k_B = -0.44 \pm 0.01$ K.

The magnetic specific heat data (Figure 13) show a pronounced λ-type anomaly, the maximum occurring at $T_c = (0.480 \pm 0.015)$ K.[47] This is quite close to the value deduced from the susceptibility experiments.

Because of the observed anisotropy in the susceptibility, as well as the crystallographic considerations, the 2-D Ising model was applied in analyzing the contribution to the specific heat coming from the cooperative magnetic transition. For this model the heat capacity has been solved by Onsager[48] for a 2-D rectangular lattice with $S = {}^1/_2$ and for an arbitrary ratio of the parameters J and J' giving the interactions between neighboring spins in the two spatial directions of the 2-D network. The theoretical curve considered above for the susceptibility in Figure 12 corresponds to the particular case $J = J'$, a quadratic lattice.

Notwithstanding the apparent agreement between experiment and theory in Figure 12 the specific heat data could not be fit with the same quadratic Ising model.

In view of the inequivalent superexchange paths in the *ab* planes, as discussed above, the ratio J'/J was then used as an adjustable parameter in the Onsager

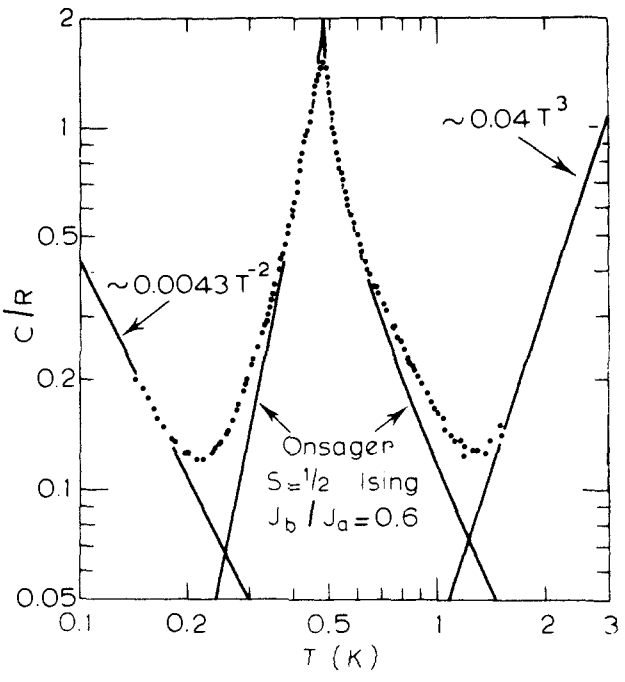

Figure 13. The magnetic specific heat of $[Co(\gamma\text{-}CH_3\text{-}C_5H_4NO)_6](ClO_4)_2$, fitted to the prediction for the rectangular Ising model with $J_a/k_B = -0.55$ K and $J_b/J_a = 0.6$. Reproduced with permission from ref 47. Copyright 1981 Elsevier, Amsterdam.

solution for the specific heat. As shown in Figure 13 the best fit with the experiment was found for a value $J'/J = 0.6 \pm 0.1$. The lattice contribution comes out as $C_{lat}/Nk_B = aT^3$, where $a = 0.04 \pm 0.01$ K^{-3}. After subtraction of this lattice term as well as the nuclear hyperfine term from the raw data, the results shown in Figure 13, fitted to the Onsager prediction with $J'/J = 0.6$ and $J/k_B = -0.55 \pm 0.02$ K, are obtained. The susceptibility for the rectangular Ising model has been calculated by Tanaka and Uryû[49] for an arbitrary ratio J'/J. Thus a fit of the same $\chi_{c'}$ data to their prediction for the case $J'/J = 0.6$ was found to yield the parameters $g_{c'} = 5.48$ and $J/k_B = -0.54$ K. The fit is of similar quality as that in Figure 12. This happens because, for values of J'/J which are not too small (i.e., >0.5), the shape of the susceptibility curve is fairly insensitive to this ratio.

The striking difference between the magnetic behavior of $[Co(\gamma\text{-}CH_3\text{-}C_5H_4NO)_6](ClO_4)_2$ and the related $[Co(C_5H_5NO)_6]X_2$ compound amounts therefore to the change from a 3-D simple cubic XY antiferromagnetic lattice into a 2-D rectangular Ising antiferromagnet, in agreement with the crystallographic information about the superexchange paths. In our opinion the above comparison provides a beautiful example of the importance of magneto-structural correlations. It is further of interest to note that the observed value of J/k_B is nearly a factor of two larger than that observed in the related compound $[Co(C_5H_5NO)_6](ClO_4)_2$, although the interatomic distances in the Co–O---O–Co superexchange bonds are in fact similar along the a-axis in $[Co(\gamma\text{-picoline } N\text{-oxide})_6](ClO_4)_2$ and even considerably larger (the O---O distance) for the path along the b axis.

3. Five-Coordinate Cobalt(II)

The crystal structure of $[Co(\alpha\text{-}CH_3\text{-}C_5H_4NO)_5](ClO_4)_2$ was reported some time ago;[50] the ligand is 2-picoline N-oxide. The material crystallizes in the monoclinic space group $P2_1/c$ with four molecules in the unit cell. The lattice consists of well-separated pentakis(2-picoline N-oxide)cobalt(II) ions and perchlorate ions. The coordination about the cobalt atom is essentially trigonal bipyramidal with the axial Co–O bond length greater than the equatorial bond length by 0.123 Å.

Some EPR studies of the polycrystalline material as well as of the compound doped into its zinc isomorph have been reported.[51] The crystal g-values are reported as $g_1 = 1.86$, $g_2 = 3.52$ and $g_3 = 5.67$; these have been transformed into the molecular g-values $g_\parallel = 2.03$ and $g_\perp = 2.38$. The zero-field splitting of the $^4A_2$ ground state has been estimated as 25 cm^{-1} (36 K).[52]

The substance appears to be paramagnetic down to a temperature of 40 mK. The 2-methyl group on the ligand forces the picoline N-oxide to be oriented such that the required Co–O---O–Co superexchange paths do not exist in this material. A comparison, then, of the magnetic properties of $[Co(C_5H_5NO)_6](ClO_4)_2$, $[Co(\gamma\text{-}CH_3\text{-}C_5H_4NO)_6](ClO_4)_2$ and of $[Co(\alpha\text{-}CH_3\text{-}C_5H_4NO)_5](ClO_4)_2$ shows, as if any further proof were needed, the importance of this superexchange path for magnetic interactions in the pyridine N-oxide compounds.

4. Bimetallic Compounds

A quite different series of cobalt compounds which contain pyridine N-oxide has also been recently[53] investigated. The parent compound is of stoichiometry $Co(C_5H_5NO)_3Cl_2$, but crystal structure analysis showed that it should be formulated as $[Co(C_5H_5NO)_6](CoCl_4)$. The compounds therefore contain two magnetic subsystems, that of the octahedral cations and that of the tetrahedral anions. Since the crystal field splittings of the cobalt in the two sites are substantially different, one might expect rather complex magnetic ordering. The compound $[Co(C_5H_5NO)_6](ZnCl_4)$ could also be prepared, and it was found to be isostructural to the Co/Co compound. This is important because the magnetic study of the Co/Zn system helped in deciphering the magnetic properties of the Co/Co compound. The measurements showed that the Zn atoms enter the lattice highly preferentially, residing only on the tetrahedral positions. Finally, the analogous bromide compounds $[Co(C_5H_5NO)_6](CoBr_4)$ and $[Co(C_5H_5NO)_6](ZnBr_4)$ were also prepared and shown to be isostructural to the chloride analogues. The compounds behave similarly, which gives further credence to the analysis of the chloride salts.

All the compounds are monoclinic and belong to the space group Cc. Superexchange paths of the familiar kind, Co–O---O–Co, are found in each of the three crystallographic directions, but no efficient Co–Cl---Cl–Co paths are evident in the crystal structure analysis.[53]

Specific heat data on $[Co(C_5H_5NO)_6](CoCl_4)$ and $[Co(C_5H_5NO)_6](ZnCl_4)$ are displayed in Figure 14. The sharp anomalies occurring near 1 K may be attributed to a magnetic ordering of the octahedral cobalt ions, since that is the only magnetic contribution observed for the Co/Zn compound. The transition temperature, 0.95 K, is the same for both compounds, and thus one must conclude that there are two uncoupled magnetic subsystems in $[Co(C_5H_5NO)_6](CoCl_4)$. The Co/Co

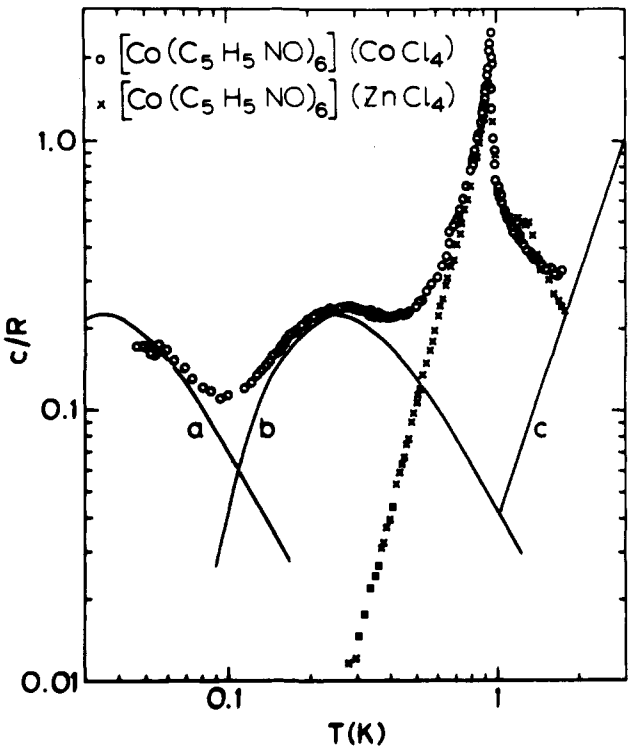

Figure 14. Specific heats of $[Co(C_5H_5NO)_6](CoCl_4)$ (○) and $[Co(C_5H_5NO)_6](ZnCl_4)$ (×). Curves (a) and (b) are the Schottky curves, while curve (c) is the estimated lattice contribution. Reproduced with permission from ref 53. Copyright 1984 Elsevier, Amsterdam.

system exhibits additional paramagnetic contributions at low temperatures which are absent in the zinc analogues, and these have been attributed to the cobalt ions at the tetrahedral sites. These are Schottky anomalies, due to the zero-field splitting of the ground state. Similar results were obtained for the bromide analogues.

These interpretations are confirmed by the susceptibility measurements, which are displayed in Figure 15 for $[Co(C_5H_5NO)_6](CoCl_4)$. The most prominent feature in the data is the large spike in the *b*-axis data at 0.94 K, which is indicative of weak ferromagnetism. The susceptibilities of $[Co(C_5H_5NO)_6](ZnCl_4)$, Figure 16, are somewhat similar, weak ferromagnetism once again being observed parallel to the *b* axis. The peak occurs at the same temperature of 0.94 K. The preferred axis of spin alignment is the *a* axis, while the *c* axis is a perpendicular axis. These features are more readily apparent in the data on the Co/Zn compound than in those on the Co/Co one because in the latter there is the additional strong paramagnetic contribution from the tetrahedral $(CoCl_4)^{2-}$ ions. The fact that the ordering anomalies in the specific heat curves of the Co/Zn compound are nearly as sharp as for the Co/Co salt and occur at precisely the same transition temperature provides strong evidence that in the Co/Zn system the preference of the zinc atoms for the tetrahedral sites is nearly 100%.

The general features of the specific heats and susceptibilities of the bromide analogues are similar, with the exception that weak ferromagnetism is not observed. The data suggest that the discrimination of the zinc for occupation of the tetrahedral sites is not as great as with the chlorides. The ordering temperature is 0.65 K for both.

The subsystems involving the tetrahedral cobalt ions

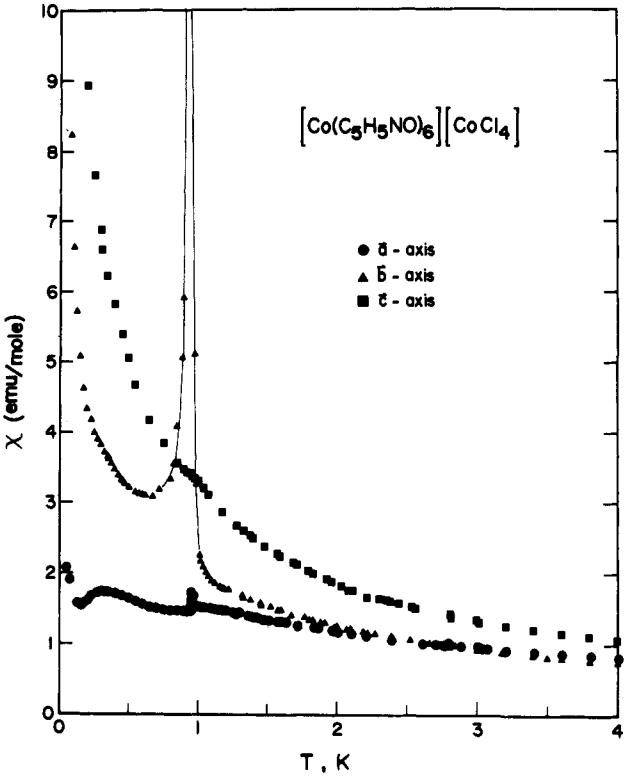

Figure 15. Susceptibility data parallel to the three crystallographic axes of $[Co(C_5H_5NO)_6](CoCl_4)$. The maximum value of χ as measured in the *b* direction at T_c is about 100 emu/mol. Reproduced with permission from ref 53. Copyright 1984 Elsevier, Amsterdam.

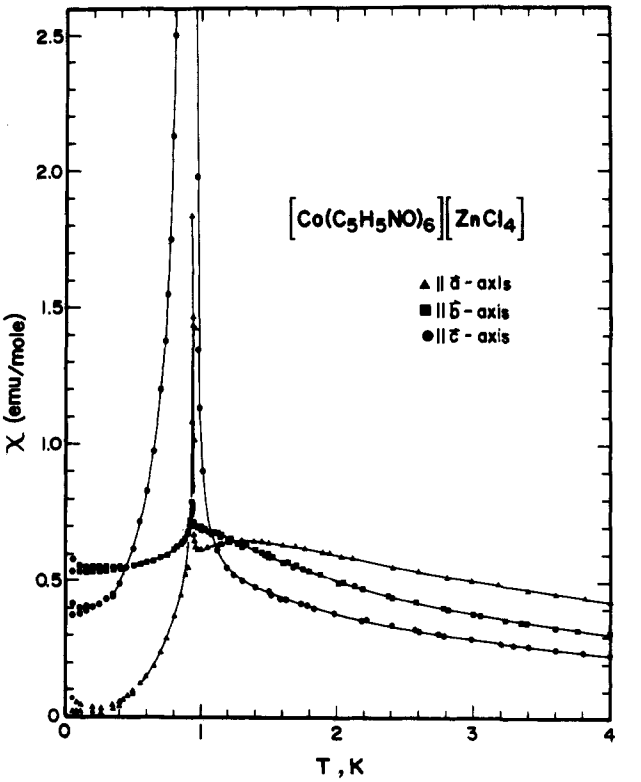

Figure 16. Susceptibility data parallel to the three crystallographic axes of $[Co(C_5H_5NO)_6](ZnCl_4)$. Note the change in the vertical scale compared to Figure 15. The maximum value of χ as measured in the *b* direction at T_c is about 100 emu/mol. Reproduced with permission from ref 53. Copyright 1984 Elsevier, Amsterdam.

do not undergo a magnetic phase transition down to 40 mK.

D. Nickel(II)

Magnetic ordering occurs with the $[Ni(C_5H_5NO)_6]X_2$ series of compounds, but in a rather unusual fashion. It has already been pointed out that, because of the large positive ZFS, these salts cannot order spontaneously. That is, no antiferromagnetic ordering occurs in zero applied field as the substances are cooled.

Indeed, the sign of D may have important implications for the low-temperature properties of nickel salts, in particular, concerning the ability of these salts to undergo long-range magnetic ordering.[30,38,54] If D is negative, the ground state is magnetic and the exchange interaction J between the neighboring ions will always lead to magnetic ordering at some sufficiently low temperature, irrespective of the magnitude of $|D/J|$. If, however, D is positive, the nonmagnetic singlet state is lowest and all the spin entropy can be removed on cooling without the necessary intervention of long-range magnetic ordering processes. This has been discussed quantitatively by Moriya,[55] using molecular field theory, who shows that a necessary condition for a nonzero critical temperature or Neel point is that D be smaller than $2zJ$, where z is the magnetic lattice coordination number. The situation that pertains to the $[Ni(C_5H_5NO)_6]X_2$ series is a positive $D > |2zJ|$, so that in zero field no ordering occurs.

On the other hand, the application of a sufficiently large external field parallel to the symmetry axis can cause the lower doublet level to cross the singlet at some critical field $H_c \simeq D/g\mu_B$. At that level-crossing field, the ground state has become an effective doublet and so ordering can occur at some temperature. The unusual feature of the $[Ni(C_5H_5NO)_6]X_2$ series of salts is that all the stringent requirements for such field-induced ordering are met, that is, (a) large, positive zero-field splitting, (b) high-symmetry crystal structure with all nickel ions equivalent (so that the applied field can be set parallel to the z-axes of all the constituent complexes), (c) level crossing field experimentally accessible, and (d) strong enough exchange interactions so that ordering occurs within an accessible temperature range. Susceptibility and specific heat measurements show that both $[Ni(C_5H_5NO)_6](ClO_4)_2$[27] and $[Ni(C_5H_5NO)_6](NO_3)_2$[16] meet all these restrictions, while it appears that $[Ni(C_5H_5NO)_6](BrO_3)_2$ meets only the first three requirements.[17]

In addition to the zero-field specific heat curve shown in Figure 4, the specific heat of $[Ni(C_5H_5NO)_6](ClO_4)_2$ was measured as a function of field applied parallel to the rhombohedral axis of the system.[56] The resulting specific heat curves for $30 < H < 60$ kOe are shown in Figure 17. It is seen that in such a linear plot, there is at first sight a nice symmetry around $H = H_{max}$, namely those curves for which the difference $H - H_{max}$ has the same absolute value but opposite sign, are quite similar in shape. However, it is apparent that this symmetry is far from being complete. The asymmetry is due to the influence of the upper $|+1\rangle$ level. The field H_{max} (or H_c, the crossing field) is found to be about 48 kOe.

Note from this figure that magnetic ordering still occurs (a λ-like peak is observed) even as the applied field moves away from H_c, but that the ordering occurs at a lower temperature. That is, there is still a mixing of the levels as the field moves away from H_c. This is

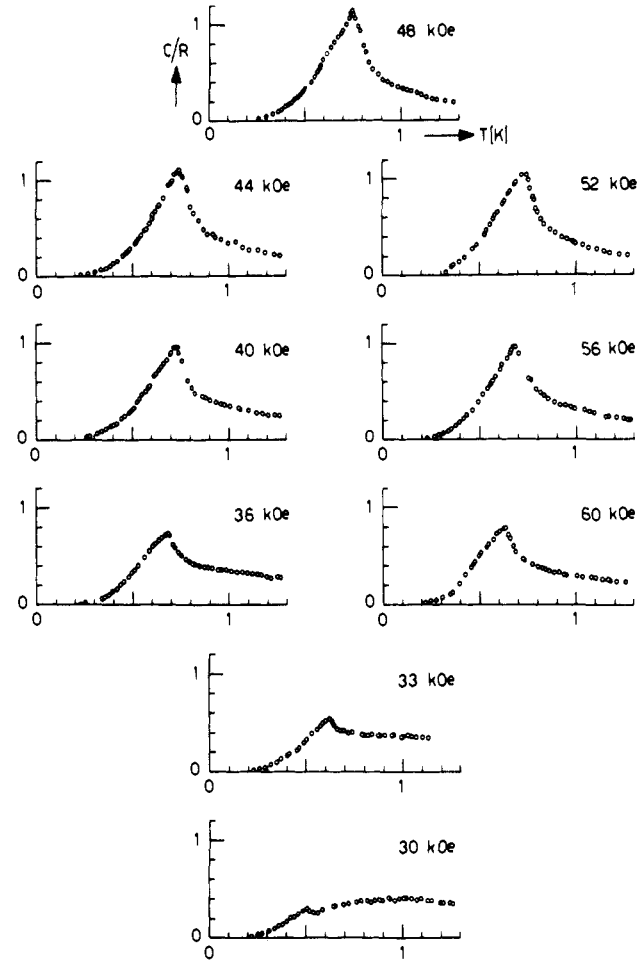

Figure 17. Linear plot of the specific-heat curves of $[Ni(C_5H_5NO)_6](ClO_4)_2$ as a function of temperature in various external fields. For each plot the vertical and horizontal scales refer to C/R and T (in K), respectively. Reproduced with permission from ref 56. Copyright 1978 Elsevier, Amsterdam.

illustrated schematically in the phase diagram in Figure 2c, where the long-range order can be seen to be established at lower and lower temperatures as H moves away from H_c. The experimentally determined phase diagram for $[Ni(C_5H_5NO)_6](ClO_4)_2$ is shown in Figure 18. The points are experimental. The curve drawn through the results has a flat maximum for $T_c(H)$ with $T_{c_{max}} = 0.75 \pm 0.01$ K at $H_{max} = 48$ kOe. For the same reason mentioned above, the experimental phase diagram is asymmetric around the line $H = H_{max}$, as is exemplified by the dash-dotted curve for $H < H_{max}$, which represents the mirror image of the curve above H_{max}. Using in addition the points at $T = 0.08$ K of ref 57, we may extrapolate the experimental curve to $T = 0$, obtaining $H_{c1} = 26 \pm 1$ kOe and $H_{c2} = 70 \pm 1$ kOe for the critical fields at $T \simeq 0$.

The MF predictions in Figure 18 have been fitted to the experimental H_{c1} and H_{c2} at $T = 0$. The theoretical expressions for these fields are $g\mu_B H_{c1} = D - 2z|J|$ and $g\mu_B H_{c2} = D + 4z|J|$ for the effective $\sigma = \pm^1/_2$ formalism, and $g\mu_B H_{c1} = D(1 - 4z|J|)^{1/2}$ and $g\mu_B H_{c2} = D + 4z|J|$ for the $S = 1$ model. With the above experimental values one then obtains the combination $J/k_B = -0.20 \pm 0.01$ K, $D/k_B = 6.3 \pm 0.2$ K and $J/k_B = -0.18 \pm 0.01$ K and $D/k_B = 6.7 \pm 0.2$ K, for these models, respectively.

The phase diagram of $[Ni(C_5H_5NO)_6](NO_3)_2$ in the H-T plane has also been determined[42] by means of the field-dependent ac susceptibility measured parallel to

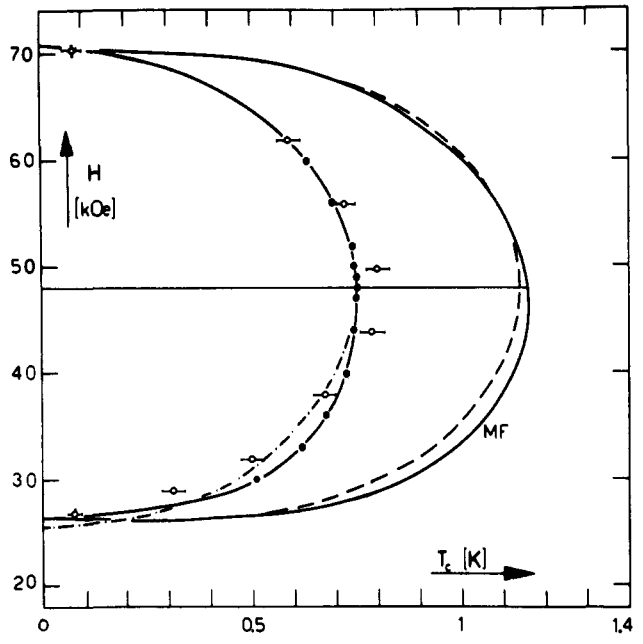

Figure 18. Magnetic phase diagram of $[Ni(C_5H_5NO)_6](ClO_4)_2$. ● from specific-heat anomalies; O data from ref 57. The dashed and solid line MF curves are for the $\sigma = \pm^1/_2$ and for the $S = 1$ model, respectively.

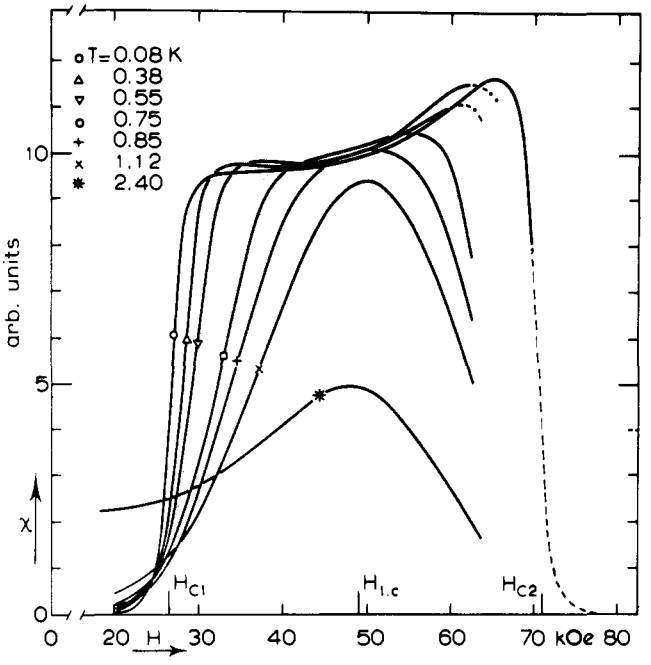

Figure 19. Field dependence of the susceptibility of $[Ni(C_5H_5NO)_6](NO_3)_2$ at several temperatures. Reproduced with permission from ref 42. Copyright 1980 Elsevier, Amsterdam.

the applied field along several adiabatics. These data are illustrated in Figure 19. The temperatures of the measurements are listed in the figure. The asymmetry of the $\chi(H_{eff}, T)$ curves and the phase diagram with respect to the level crossing field originates from the field-dependent mixing of the energy levels due to the exchange interactions. It is striking that all the curves of $\chi(H_{eff}, T)$, neglecting the above mentioned asymmetry, are comparable with the field and temperature dependence of the perpendicular susceptibility of a normal 3-D antiferromagnet. This was expected as the susceptibility was measured along the z axis, which, under these particular conditions, is perpendicular to the spontaneous magnetization in the ordered state.

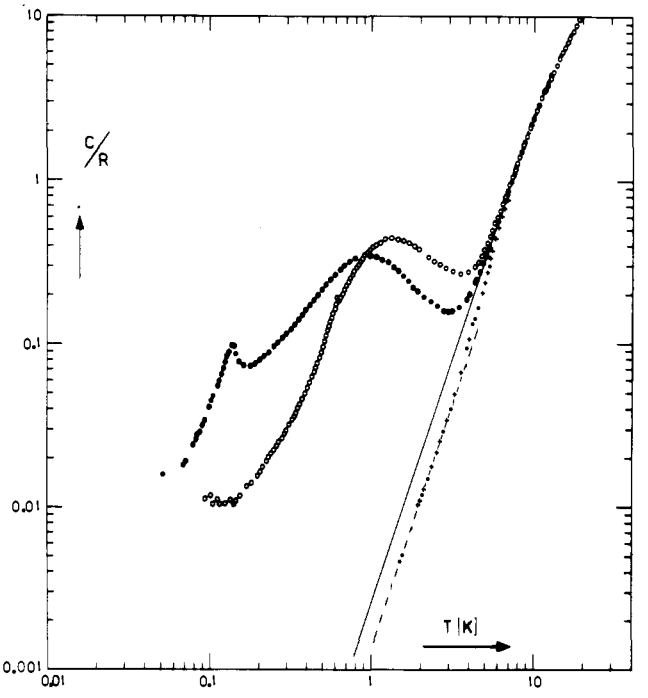

Figure 20. Double logarithmic plot of the specific-heat data obtained for (O) $[Cu(C_5H_5NO)_6](BF_4)_2$; (●) $[Cu(C_5H_5NO)_6](ClO_4)_2$, and (+) $[Zn(C_5H_5NO)_6](BF_4)_2$. The curves are discussed in the text. Reproduced with permission from ref 33. Copyright 1978 Elsevier, Amsterdam.

E. Copper(II)

The magnetic behavior of the $[Cu(C_5H_5NO)_6]X_2$ series of compounds is controlled, at low temperatures, by the Jahn–Teller effect.

The specific heat results for the perchlorate and the fluoborate[33] are displayed in Figure 20, which clearly illustrates the striking differences between the behavior of the two compounds from that of the other materials discussed earlier. The measurements on the zinc sample provide an estimate of the lattice contribution in addition to the one already shown in Figure 4.

In contrast to the 3-D magnetic behavior found for the other compounds, the magnetic specific heat of $[Cu(C_5H_5NO)_6](ClO_4)_2$ is found to be excellently described by the Bonner–Fisher[58] prediction for a $S = {}^1/_2$ antiferromagnetic Heisenberg *chain*. The fit yields an intrachain exchange constant of $J/k_B = -1.02 \pm 0.02$ K. Weak interchain interactions lead to the onset of long-range 3-D magnetic order at $T_c = 0.142 \pm 0.002$ K. Below T_c, the experimental specific heat is found to be well represented by the sum of a T^3 dependence and the expected T^{-2} dependence arising from the hyperfine interactions. As regards the T^3 term, such a steep fall of the specific heat below T_c is usually observed in quasi-linear-chain compounds.[1]

When these experiments were performed, the observation of 1-D magnetic behavior came rather as a surprise in view of the previous studies on the other compounds. However, we were in for even more surprises. Although the magnetic specific heat of $[Cu(C_5H_5NO)_6](BF_4)_2$ also shows a broad maximum, the shape is quite different and it was found to be in good agreement with predictions obtained for the 2-dimensional quadratic *layer* $S = {}^1/_2$ Heisenberg antiferromagnet.[59] The fit of the high temperature series prediction to the experiment yields $J/k_B = -1.10 \pm 0.05$

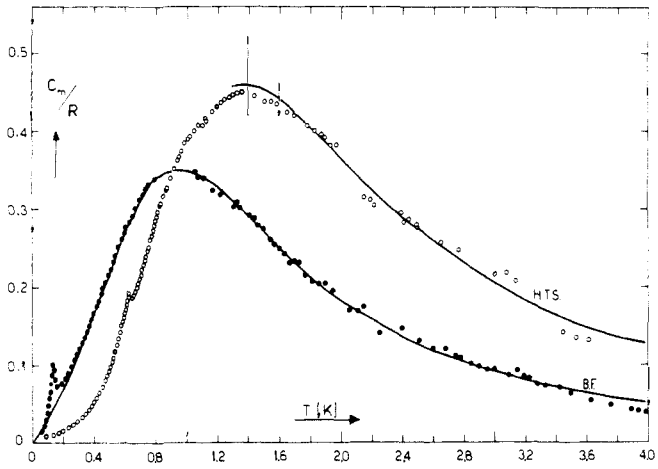

Figure 21. Comparison of the magnetic specific heats for $[Cu(C_5H_5NO)_6](ClO_4)_2$ and $[Cu(C_5H_5NO)_6](BF_4)_2$ (● and ○, respectively) plotted on a linear scale. Curve B–F is the Bonner–Fisher[58] prediction for a linear chain antiferromagnet with $J/k_B = -1.02$ K; curve H.T.S. is the prediction from the high-temperature series for the quadratic-layer antiferromagnet with $J/k_B = -1.10$ K. Reproduced with permission from ref 33. Copyright 1978 Elsevier, Amsterdam.

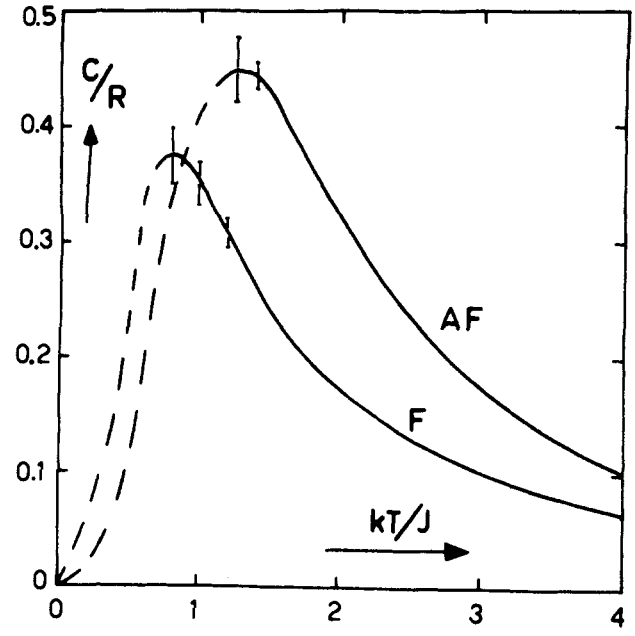

Figure 22. Specific heat curves for the antiferromagnetic (AF) and ferromagnetic (F) quadratic-layer Heisenberg lattices. Reproduced with permission from ref 33. Copyright 1978 Elsevier, Amsterdam.

K for the intralayer exchange.

The powder susceptibilities of the two salts have also been measured and the observed broad maxima confirm the 1-D and 2-D magnetic behavior, respectively, found from the heat capacities.[33]

It thus appeared that the ClO_4^- compound behaves like a linear chain system, whereas the BF_4^- compound apparently approximates the quadratic Heisenberg layer. This, despite the fact that the two substances are isostructural at room temperature with one another and with the other compounds of the series! The magnetic specific heats of the two compounds are shown in a linear plot in Figure 21. We mention in particular that the results for $[Cu(C_5H_5NO)_6](BF_4)_2$ show very clearly that the specific heat of the quadratic layer Heisenberg antiferromagnet will have the form of a nonsingular curve, with a broad maximum of height $C/R \simeq 0.45$ at $k_BT/|J| \simeq 1.3$. In this respect they provide an interesting extension of the work of Bloembergen[60] on the series of compounds $(C_nH_{2n+1}NH_3)_2CuX_4$ (n = 0, 1, 2, 3, ...; X = Cl, Br), which have been shown to be very good examples of the ferromagnetic Heisenberg layer.[1] From his experiments Bloembergen was able to derive an estimate for the specific heat for this model, which is compared with the result for $[Cu(C_5H_5NO)_6](BF_4)_2$ in Figure 22. For the ferromagnetic layer the maximum in C/R is lower ($C_{max}/R \simeq 0.38$) and occurs at a lower temperature ($kT_{max}/J \simeq 0.8$) than for the antiferromagnetic case ($C_{max}/R \simeq 0.45$; $k_BT_{max}/|J| \simeq 1.3$).

As a possible explanation, we have pointed out[33] that the lower dimensional properties of both compounds should be ascribed to the occurrence of (static) Jahn–Teller distortions of the oxygen octahedra surrounding the Cu^{2+} ions. The packing of the distorted octahedra should then be different in the two salts, since they must lead to a lack of overlap in one and in two spatial directions for $[Cu(C_5H_5NO)_6](BF_4)_2$ and $[Cu(C_5H_5NO)_6](ClO_4)_2$, respectively.

A quite similar phenomenon has in fact been observed earlier in the perovskite structure, where compounds like $RbMnF_3$ and $KNiF_3$ are simple cubic antiferromagnets whereas $KCuF_3$ is a quasi 1-D antiferromagnet.[1] It has been proved that the 1-D properties are due to static Jahn–Teller distortions in $KCuF_3$, leading to a lack of overlap of cation and anion wave functions in the plane perpendicular to the c axis, as shown in Figure 23. Our predictions for the pyridine N-oxide compounds of copper have been verified by

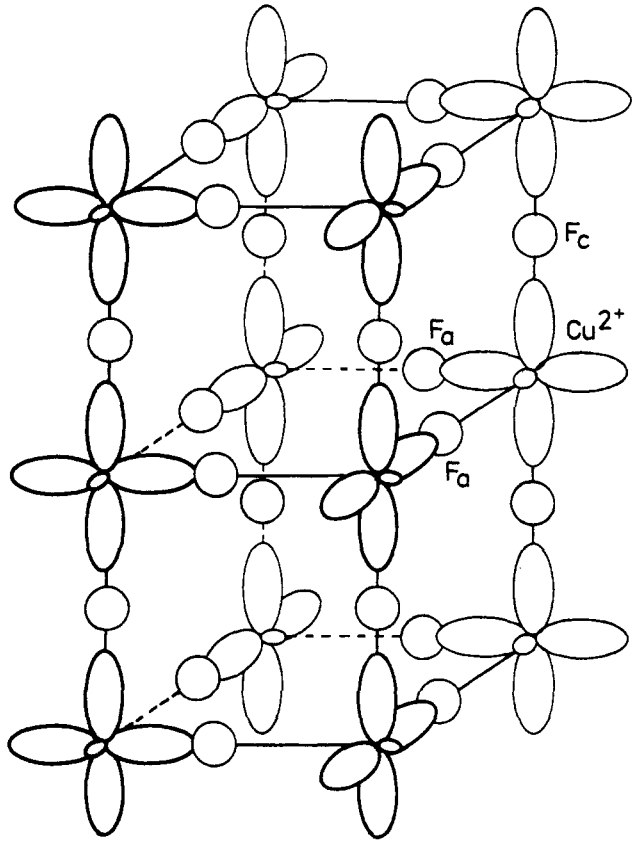

Figure 23. Alignments of the e_g orbitals of the copper ions in $KCuF_3$. The one-dimensional behavior arises because there is hardly any overlap of the wave functions along the a axes.[1]

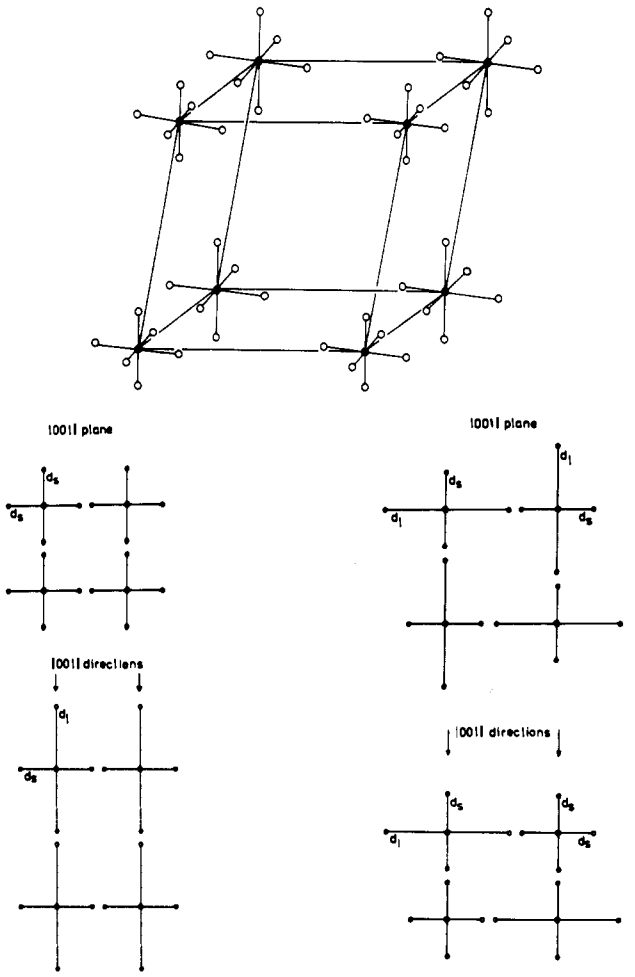

Figure 24. (a) Simplified structure of the $[M(C_5H_5NO)_6]X_2$ compounds, showing the M^{2+} ions at the corners, octahedrally surrounded by the oxygen atoms (open circles), (b) ferrodistortive, and (c) antiferrodistortive order of the elongated CuO_6 octahedra in $[Cu(C_5H_5NO)_6](BF_4)_2$ and $[Cu(C_5H_5NO)_6](ClO_4)_2$, respectively. The symbols d_l and d_s denote the long and short Cu–O bonds, respectively.[61,62]

Reinen and Krause.[61] From EPR experiments these authors deduced that the packing of the tetragonally elongated octahedra is ferrodistortive and antiferrodistortive for $[Cu(C_5H_5NO)_6](BF_4)_2$ and $[Cu(C_5H_5NO)_6](ClO_4)_2$, respectively, as shown in Figure 24. The antiferrodistortive packing is of course quite similar to what has been found in $KCuF_3$, the difference being that in $[Cu(C_5H_5NO)_6](ClO_4)_2$ the octahedra are *isolated* from each other, whereas in $KCuF_3$ they share corners. Since the e_g orbitals of the copper ion are directed only towards the short Cu–O distances, it is evident that for the fluoborate and the perchlorate compound there will be an appreciable overlap of wave functions only in the (001) plane and along the [001] axis respectively, explaining the observed magnetic characteristics. Lastly, the remarkable experimental feature[33] that the *intrachain* exchange (J/k_B = −1.02 K) for $[Cu(C_5H_5NO)_6](ClO_4)_2$ is so nearly equal to the *intralayer* exchange (J/k_B = −1.10 K) found for $[Cu(C_5H_5NO)_6](BF_4)_2$, is also nicely explained by the EPR studies. Since the superexchange interaction is extremely sensitive to the interatomic distances of the bridging atoms, it would follow that the Cu–O---O–Cu bonds connecting the copper moments into chains or layers should be very nearly equal. Indeed, as regards the extent of the static distortions the EPR measurements yield nearly the same g values for the short (1.98–1.99 Å) and long (2.29–2.30 Å) Cu–O distances in both compounds (the Cu–Cu distances are also nearly the same, namely 9.60–9.63 Å for both materials).

We remark that $[Cu(C_5H_5NO)_6](BF_4)_2$ is to our knowledge the first good example of a quadratic-layer Heisenberg antiferromagnet with a spin value as low as $^1/_2$ (copper compounds tend to be ferromagnetic).[62] The pronounced quantum effects that should occur make this an interesting compound for further studies. The single-crystal susceptibilities have been measured[63a] over the temperature interval 40 mK–4.2 K by Burriel and analysed in part by Navarro.[63b] The data do not exhibit a macroscopic easy axis, probably because of the different local orientations of the Jahn–Teller-elongated octahedra. There may also be several crystallographic domains. The data therefore cannot be analyzed in detail. As an example of the two-dimensional character, we mention that the coefficient a in the aT^2 term describing the magnetic specific heat at the lowest temperatures exceeds by far the prediction from noninteracting spin-wave theory.[59] At this moment the high-temperature series (H.T.S.) expansion for the specific heat of the quadratic layer Heisenberg antiferromagnet, complemented by our results for $[Cu(C_5H_5NO)_6](BF_4)_2$, appear to be the most complete estimate for the specific heat of this model. Similar considerations apply in case of the quadratic layer Heisenberg ferromagnet, where the H.T.S. prediction is nicely confirmed by the results[62] for $Cu(NCS)_2(triazole)_2$, and is at low temperatures complemented by the results of Bloembergen[60] on the series of compounds $(C_nH_{2n+1}NH_3)_2CuCl_4$ (n = 1 to 10). Both these results present a challenge for complete theoretical verification.

As another more general conclusion arising from the work on the pyridine *N*-oxide compounds and the earlier results on $KCuF_3$, it transpires that, in case of a highly symmetric crystal structure with collinear exchange paths, one will end up with a low-dimensional magnetic system as soon as a Jahn–Teller ion such as Cu^{2+} or Cr^{2+} is taken for the metal atom. This conclusion has been confirmed by the work of Blöte on the hexanitrocuprates,[64] which also show 1-D or 2-D magnetic behavior although the undistorted lattice would be fcc.

F. Mixed and Diluted Systems

The magnetic matrix lattice provided by the $[M(C_5H_5NO)_6]X_2$ system also proves to be of interest for physical problems quite different from those described above. This arises from the fact that this matrix allows the mixing of different 3d metal atoms. If two different magnetic metal atoms are concerned (e.g., Co^{2+} and Fe^{2+}) we will speak of mixed magnetic compounds, while if a magnetic and a nonmagnetic metal atom (e.g., Co^{2+} and Zn^{2+}) are involved, we will speak of magnetically diluted systems. The latter problem, which we shall discuss first, bears directly on percolation phenomena, which are of importance for many fields of physics as well as for other sciences.[3] A very attractive physical realization of the percolation phenomenon is in fact the site-random diluted magnet, where in a magnetic compound the magnetic atoms are replaced randomly by nonmagnetic ones in increasing amounts through doping with a diamagnetic isomorph.[65,66] If p

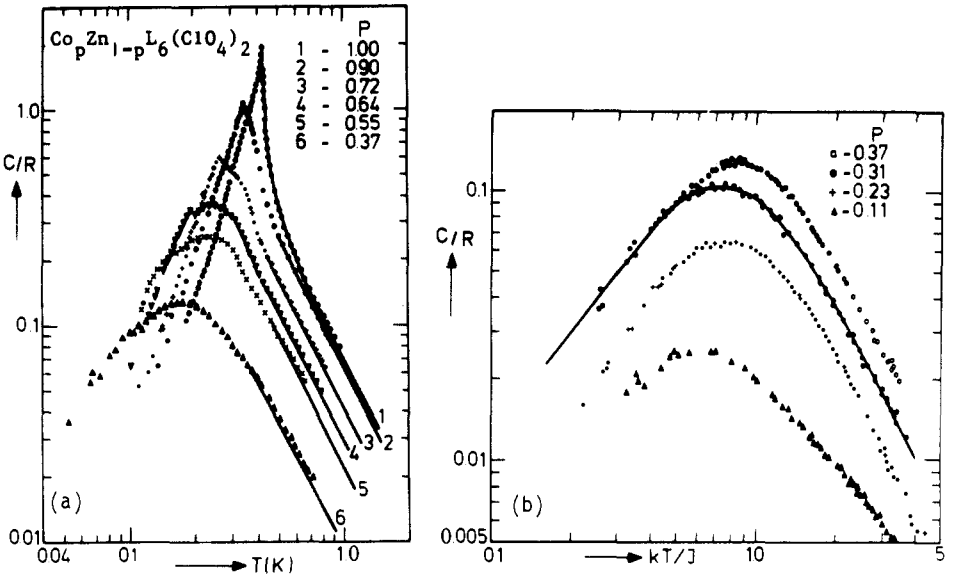

Figure 25. (a) Magnetic specific heat for $[Co_pZn_{1-p}(C_5H_5NO)_6](ClO_4)_2$ for $p \geq 0.37$. Curves drawn are explained in the text. (b) As in (a), but for $p \leq 0.37$. The solid curve is the prediction for the antiferromagnetic chain with $\alpha = 0.31$. Reproduced with permission from ref 69. Copyright 1979 American Institute of Physics.

is the fraction of magnetic ions, where $p = 1$ and $p = 0$ correspond to the purely magnetic and nonmagnetic limits, the magnetic ordering temperature T_c will decrease with p and at a critical concentration p_c its value will be reduced to zero. For loose-packed 3-D lattices p_c is equal to the percolation threshold (critical probability) of the corresponding site percolation problem. For $p < p_c$, only finite isolated clusters of magnetic atoms exist with the average cluster-size diverging at p_c, marking the onset of the formation of the infinite percolation cluster (IPC) of magnetic atoms for $p \geq p_c$. The presence of the IPC is a necessary condition for the occurrence of long-range magnetic order. As p is increased above p_c the fraction $n(p)$ of spins in isolated clusters drops quite rapidly, since they coalesce with the IPC. Numerical estimates for the s.c. lattice,[67] for which $p_c = 0.31$, yield $n(p) \simeq 5$ % and 0.7 % for $p = 0.39$ and 0.58, respectively. We may conclude that for $p > 1.2$ p_c, the magnetic behavior of the diluted magnet will be dominated by the properties of the IPC. Thus experimental studies of this behavior supply direct information on the thermodynamics of the IPC, and since this is expected theoretically to be an object of "*fractal* dimensionality", such studies are of current interest.

Several experiments have been carried out[68-70] in which the cobalt ion in $[Co(C_5H_5NO)_6](ClO_4)_2$ has been partially replaced by the diamagnetic zinc ion. The system $[Co_pZn_{1-p}(C_5H_5NO)_6](ClO_4)_2$ is ideal for specific-heat studies of a diluted magnet for the following reasons. Firstly, the magnetic ordering occurs at temperatures low enough for the lattice specific heat to be negligible, but, on the other hand, still accessible by a conventional adiabatic demagnetization cooling apparatus. Secondly, the magnetic exchange does not vary appreciably with dilution because the Co and Zn compounds have nearest-neighbor distances equal within 0.1%. These properties follow from the large separation of the metal ions (~9.5 Å), and from the fact that they are "encaged" in a surrounding of six C_5H_5NO ligands, so that the lattice is insensitive to the particular 3d metal ion chosen. Thirdly, powdered samples of the mixed materials are relatively easy to prepare in any

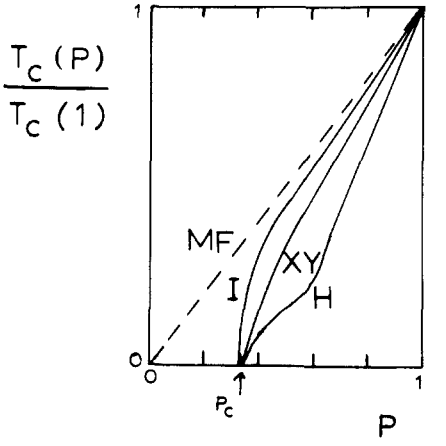

Figure 26. Qualitative dependence on p of the magnetic ordering temperature of 3-D ferromagnets (I = Ising; H = Heisenberg).

desired ratio and with *random* mixing. Indeed, it was found that the observed coefficients of the high-temperature T^{-2} term of the specific-heat curves for the mixed compounds vary as p^2. This is one of the few means available to prove experimentally that one is dealing with randomly diluted systems and not with mixtures of the separate (Co and Zn) phases. In the latter case T_c would remain at the same position, and the T^{-2} tail would vary as p.

Specific heat results for a number of p values are displayed in Figure 25. The specific heat curves for $p < 0.7$ are composed of a broad anomaly, characteristic for short-range order contributions, plus a small, λ-type, long-range order peak at $T_c(p)$. With decreasing p, the amplitude of this peak is considerably reduced and it becomes experimentally no longer observable for $p < 0.5$. As shown in Figure 26, the plot of $T_c(p)$ vs. p appears to extrapolate well to the critical concentration (percolation limit) $p_c = 0.31$ for which one should have $T_c(p_c) = 0$. The experimental points are rather well described by the variation of $T_c(p)$ predicted by the s.c. XY model.

We show in Figure 25b representative experimental curves for samples with $0.11 \leq p \leq 0.37$. Here the

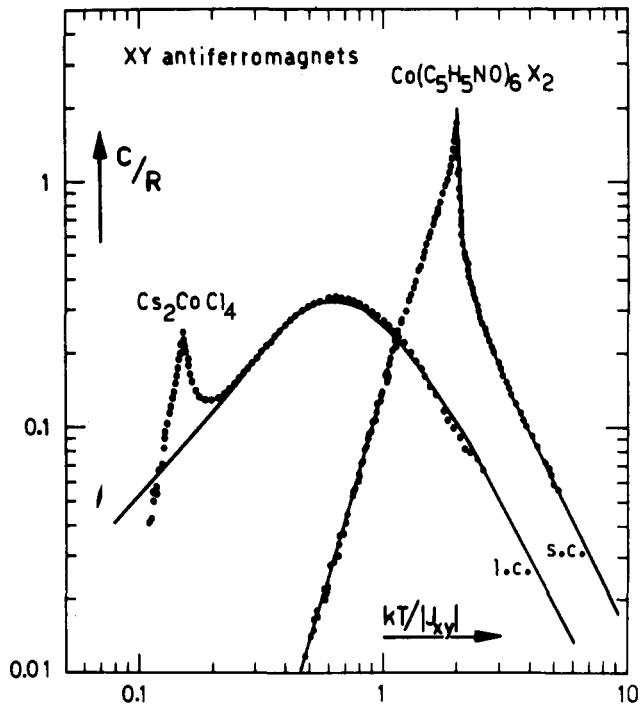

Figure 27. Magnetic specific heats of XY systems ($S = {}^1/_2$). Solid curves labelled s.c. and l.c. are theoretical predictions for the simple cubic and linear-chain XY models, respectively.

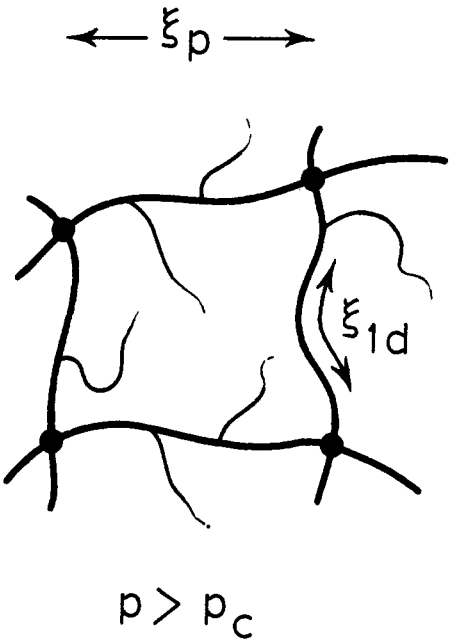

Figure 28. The structure of the infinite cluster according to the "nodes and links" model. The nodes, which are at distances of the order ξ_p are connected by macrobonds (bold lines), which form part of the backbone of the infinite cluster. The dangling ends (light lines) are not connected to infinity. The thermal correlation length ξ_T may be correlated to the intrachain correlation length $\xi_{1d}(T)$, which behaves differently for the Ising, XY, and Heisenberg types of interaction.

relative temperature $k_BT/|J_{xy}|$ has been used, with $J_{xy}/k_B = -0.204$ K. It appears that just for $p = p_c$ the shape of the experimental specific-heat curve is indistinguishable from that of a linear-chain antiferromagnet with the same interaction Hamiltonian as the undiluted magnetic system. The solid curve through the data for $p = 0.31$ in Figure 25b represents the prediction for the antiferromagnetic chain with $J_{xy}/J_z = 3.2$. To be specific, the horizontal scale for the theoretical curve is thus fixed by the exchange constant $J_{xy}/k_B = -0.204$ K, i.e., exactly the same as obtained for the pure magnetic system, whereas only the vertical scale is adjusted to obtain a coincidence with the experiment. The multiplication factor needed for this adjustment was 0.31 (the linear-chain curve has a maximum $C_{max}/R = 0.34$), that is just equal to the concentration of magnetic ions in the sample. It is quite difficult to ascribe to mere chance the fact that precisely for $p = p_c$ the form of the curve, as well as its position on the T axis, fully agree with the linear-chain prediction. As seen in Figure 27 this is indeed not so for the other concentrations around p_c that were studied.

In qualitative respect, the specific heat curves for $p \leq 0.65$ in Figure 25a are very reminiscent of what is found experimentally[35] for a quasi 1-D XY magnet, i.e., a 3-D system of XY chains with interchain coupling J' much smaller than the intrachain interaction, J. In Figure 27 specific heat data on the $S = {}^1/_2$ XY linear chain compound Cs_2CoCl_4 are compared with those for $[Co(C_5H_5NO)_6](ClO_4)_2$. Also in the quasi 1-D magnets a dimensionality crossover occurs, since the magnetic properties at high temperatures are indistinguishable from purely 1-D behavior, whereas at low temperatures the interchain coupling J' causes a transition to 3-D behavior.[35] Superimposed upon the broad chain specific heat curve, one finds[69] at a low enough temperature a λ-peak reflecting the transition to 3-D magnetic order at T_c^{3d}. (This is precisely the effect seen also in the curves of the $Cu-C_5H_5NO$ salts in Figure 20.)

As we have already outlined elsewhere,[65,66,71] the analogies between these two physical problems, namely, the diluted 3-D magnet and the quasi-1-D magnet with weak interchain coupling, may be understood on the basis of the so-called nodes-and-links model describing the infinite cluster as $p \rightarrow p_c$. In this model,[72,73] the infinite cluster is represented by a network of 1-D macrobonds, crossing at nodes separated by distances of the order of the connectedness length ξ_p, as sketched in Figure 28. This infinite cluster is a self-similar object, meaning that its basic structure is insensitive to the length-scale by which it is looked upon.

For length scales ξ_T smaller than ξ_p, where ξ_T is the thermal correlation length, this infinite cluster will behave as an object of fractal dimensionality; for length scales $\xi_T > \xi_p$ it will behave as an ordinary 3-D system. Obviously, for $p \rightarrow p_c$ one has $\xi_p \rightarrow \infty$, so that with decreasing p, the transition from fractal to 3-D behavior occurs at an increasingly lower temperature. Most importantly, the thermal length scale ξ_T will be driven by the correlation length along the macrobond, which, since the latter is of a 1-D nature, will behave grosso modo as the intrachain correlation length ξ_{1d} of the corresponding ideal chain system with the same interaction hamiltonian.

Evidently, the macrobonds connecting the nodes of the infinite cluster are not exactly chains but have some structure which, although essentially 1-D in character, will differ the more from a single ideal chain the further p is above p_c. Thus, the shape of the broad anomalies seen in Figure 25 for $p \leq 0.7$ is not independent of p. The fact that for $p \rightarrow p_c$ the form of this anomaly is found to become well-described by the theoretical curve for an XY chain, as is shown in Figure 27 agrees quite well with the nodes-and-links model for the infinite

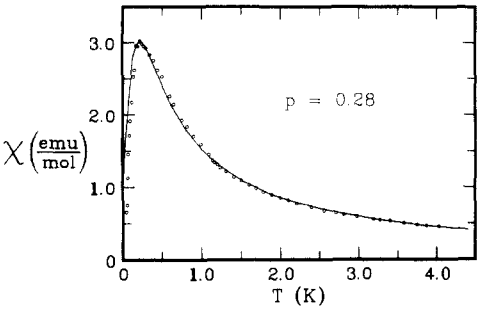

Figure 29. Susceptibility data on $[Co_pZn_{1-p}(C_5H_5NO)_6](NO_3)_2$ single crystals, for $p = 0.28$. The paramagnetic contributions of the isolated clusters have been subtracted. The solid curve corresponds to the XY, $S = {}^1/_2$ linear chain, reduced by a factor of ${}^1/_{1.22}$. Reproduced with permission from ref 63a.

cluster, since the latter will become more and more "thready" as p approaches p_c by the divergence of ξ_p. Below p_c the specific heat anomaly will just be due to the contributions from the isolated finite clusters, the average size of which is expected to diverge for $p \rightarrow p_c$, marking the onset of the infinite cluster present above p_c.

The susceptibilities of the same system are currently under investigation.[70] Some of the data are illustrated in Figure 29, where it will be seen that there is again a remarkable coincidence between experiment and the calculated behavior for a linear chain.

In another study,[71] diluted compounds of the iron salt, $[Fe_pZn_{1-p}(C_5H_5NO)_6](ClO_4)_2$ were investigated in order to study the effect of dilution of the s.c. Ising magnet. Although the physical problem of percolation is the same as for the cobalt s.c. XY analogue, the thermodynamic behavior of the infinite percolation cluster was found to be completely different. This could again be satisfactorily explained on the basis of the temperature dependence of the fundamental length scale ξ_{1d}, which drives the phase transition and which is basically different for the Ising case, where ξ_{1d} is proportional to $\exp(J/k_BT)$, as for the XY case, where ξ_{1d} is proportional to J/k_BT. As a consequence of the exponential dependence, the important short-range order effects which are seen to develop for the XY case for p values well above p_c already (Figure 25a) do not appear in the Ising case except very close to p_c.

Finally, we remark that a study on the mixed magnet $[Fe_pCo_{1-p}(C_5H_5NO)_6](ClO_4)_2$ has also been carried out.[74] Since the pure iron and cobalt salts have, respectively, Ising and XY anisotropy in the interaction (but both have $S = {}^1/_2$), one is dealing here with the problem of competing spin anisotropies. Qualitatively it may be explained as follows. The crystal field fixes the iron moments parallel to the c axis, whereas it forces the cobalt spins to lie in the plane perpendicular to it. Since the Fe^{2+}–Co^{2+} exchange is very weak compared to these crystal-field anisotropies, the iron and cobalt moments are indeed "at right angles to one another". In case the iron-cobalt interactions can be written as the dot product of spin-vectors, this interaction therefore just vanishes. One has the remarkable situation of two interpenetrating magnetic subsystems which are not magnetically interacting. The iron subsystem experiences the Co^{2+} ions as *paramagnetic* impurities, and vice versa. The two subsystems order completely independently of one another (in the range $p > p_c = 0.31$ for the Fe^{2+} subsystem and $p < 1 - p_c = 0.69$ for the Co^{2+} subsystem.) In the intermediate range $0.31 < p < 0.69$, two independent phase transitions should thus occur, which effect was however difficult to detect in the reported specific heat studies due to the smallness of the λ-anomaly for the diluted XY magnet for p values close to p_c, as discussed above.

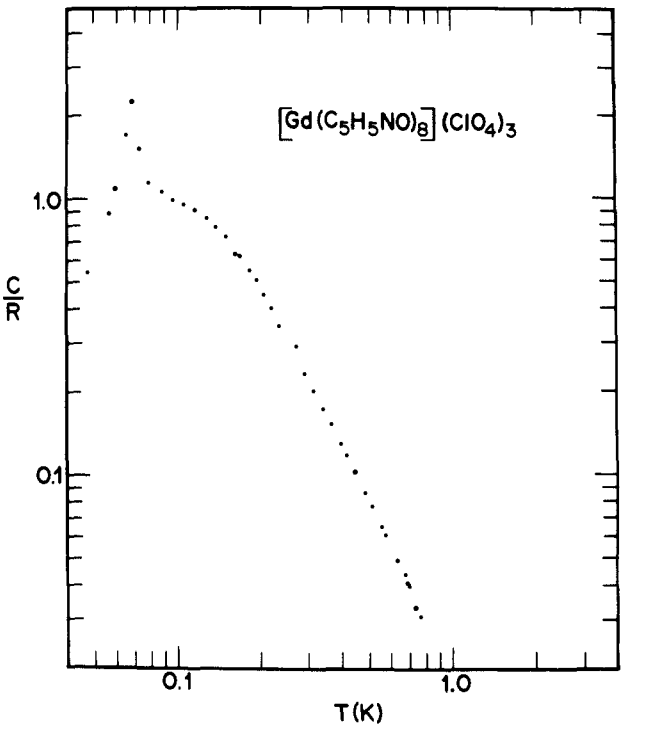

Figure 30. Specific heat of $[Gd(C_5H_5NO)_8](ClO_4)_3$. Reproduced with permission from ref 76.

G. Rare Earths

Pyridine *N*-oxide (and its derivatives) coordinates readily with the rare earths. The crystal structures of the lanthanum and neodymium salts, $[M(C_5H_5NO)_8](ClO_4)_3$, have been reported.[75] Both materials crystallize in two different monoclinic forms, space groups $P2_1/a$ and $C2/c$, and both forms contain discrete, eight-coordinate $[M(C_5H_5NO)_8]^{3+}$ ions. The coordination geometry for one form is intermediate between a cube and a square antiprism, while the second approximates the square antiprism.

Magnetic studies on several of these salts have been initiated.[76] The magnetic susceptibility of $[Gd(C_5H_5NO)_8](ClO_4)_3$ increases with decreasing temperature in a Curie–Weiss fashion, the data above 1 K being described by the parameters $\langle g \rangle = 1.98 \pm 0.01$ and $\theta = 0.046 \pm 0.05$ K for $S = {}^7/_2$. The data go through a maximum at about 80 mK, and then decrease with decreasing temperature. The antiferromagnetic ordering temperature is 70 ± 2 mK.

The specific heat results agree, a λ-anomaly being observed with maximum at 70 ± 1 mK. A shoulder on the high-temperature side of the data may be analyzed in terms of dipole–dipole interaction. The magnetic data are illustrated in Figures 30 and 31. It has also been found that $[Gd(C_5H_5NO)_8]I_3$ orders at 70 mK. The crystal structures of the gadolinium salts have not as yet been determined.

The low-ordering temperatures of the gadolinium salts illustrate as expected, that the superexchange interactions are weak in these rare-earth salts, and that

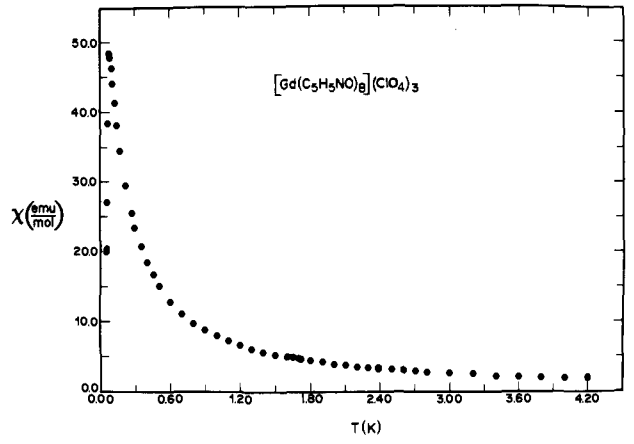

Figure 31. Magnetic susceptibility of polycrystalline $[Gd(C_5H_5NO)_8](ClO_4)_3$. Reproduced with permission from ref 76.

the long-range dipole–dipole interactions probably are the principal source of the magnetic interaction. Therefore this series of rare earth compounds should provide good examples of dipolar systems. This whole field is as yet still unexplored.

VI. Other Systems

Several other compounds with pyridine *N*-oxide as a ligand have been prepared. These include salts of the trivalent ions of chromium and iron, $[M(C_5H_5NO)_6]X_3$. The susceptibility of $[Cr(C_5H_5NO)_6](ClO_4)_3$ has been reported to obey the Curie–Weiss law over the temperature interval 1.2–4 K with the parameters $g = 1.99$ and $\theta = -0.03$ K,[77] and the EPR spectrum of the iron compound has been reported.[78] The zero-field splitting parameter D is reported as 0.36 cm^{-1}, and $\lambda = E/D = 0.233$, which suggests once again a large crystal-field distortion. Both compounds appear to be typical in their paramagnetic properties. No one has yet been successful in preparing large single crystals of either of these substances, nor has their crystal structure been reported. There are no low-temperature measurements on either compound.

There are a number of compounds with stoichiometry such as $[Cu(C_5H_5NO)X_2]_2$ and $[Cu(C_5H_5NO)_2X_2]_2$, where X is chloride or bromide, in which pyridine *N*-oxide serves as a bridging ligand between two copper ions. This provides an excellent superexchange path between the copper ions, and results in strong pairwise magnetic interaction. The molecular structure of the chloride compound is illustrated in Figure 32. The magnetic susceptibility behaves as anticipated for a dimer,[79] going through a maximum as the temperature decreases, and the data may be fit by the well-known Bleaney–Bowers equation for a mol of dimers,

$$\chi = \frac{2Ng^2\mu_B^2}{3k_BT} \cdot \frac{1}{1 + \frac{1}{3}\exp(-2J/k_BT)} \qquad (7)$$

The magnetic properties of this system change as the 4-position in the pyridine *N*-oxide ligand is substituted by other groups (nitro, methyl, etc.). The exchange constant ($-2J$) is several hundreds of Kelvins, or more.

One study[80] of interest concerns the set of dimers $[Cu(4\text{-}R\text{-}C_5H_5NO)_2(NO_3)_2]_2$, where R = H, CH_3, and OCH_3. These materials appear to be binuclear with pyridine *N*-oxide groups bridging the metal ions,[81] and

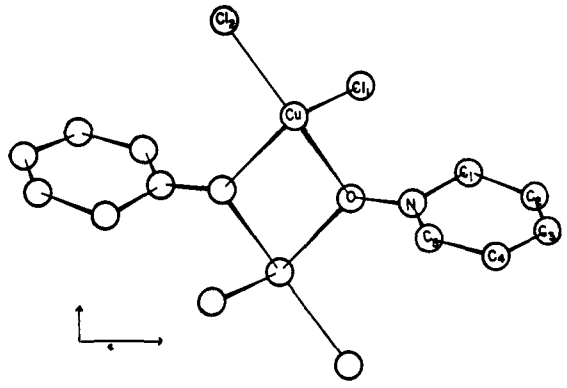

Figure 32. Molecular structure of $[Cu(C_5H_5NO)Cl_2]_2$. Reproduced with permission from ref 79. Copyright 1956 American Institute of Physics.

the nitrate ions complete the coordination sphere. The susceptibility and magnetization have been reported on powdered samples down to 1.7 K. Although there is no question about the binuclear character of these compounds, there is some controversy about the nature of the magnetic interactions. While Hatfield[82] maintains that these compounds contain spin-$^1/_2$ pairs with an $S = 1$ ground state (i.e., a ferromagnetic pair interaction of $J/k_B \simeq +7$ K), this interpretation has been shown to be wrong in subsequent studies of Carlin and coworkers.[83]

VII. Concluding Remarks

In the above we hope to have shown that notably the series of $[M(C_5H_5NO)_6]X_2$ compounds provides a remarkable set of magnetic model systems and that it yields a "magnetic matrix" comparable in value for magnetism as the well-known series of compounds AMF_3, A_2MF_4, etc., mentioned in the introduction. The investigations summarized in this paper may be considered as a preliminary survey of these materials. Quite a lot of interesting work remains to be done, both in the 3d metal pyridine *N*-oxide compounds and in the related lanthanide systems, which have only barely been investigated as yet.

Besides their contribution to our understanding of basic magnetic ordering phenomena, these materials provide us with a number of beautiful examples of magnetostructural correlations and of superexchange interactions over long distances. The interest of these types of correlations reaches far beyond physics and magnetochemistry, notably to biochemistry as has recently been outlined in a NATO–ASI.[2] Obviously, the set of interaction parameters arising from the M^{2+}–O––O–M^{2+} superexchange path for varying 3d metal ion, as obtained from these experiments, forms a challenging problem for theorists working on the calculations of superexchange interactions.

In conclusion, the present series of magnetic compounds underlines the great potential importance of coordination and organometallic chemistry for providing new and interesting materials to the solid state physicists and chemists.

VIII. Acknowledgments

RLC's research has been supported by a succession of grants, most recently DMR-8515224, from the Solid

State Chemistry Program of the Division of Materials Research of the National Science Foundation. In so far as the research cited in this review was carried out at Leiden, it was part of the research program of the "Stichting voor Fundamenteel Onderzoek der Materie," and was made possible by financial support from the "Nederlandse Organisatie voor Zuiver Wetenschaaplijke Onderzoek."

IX. References

(1) de Jongh, L. J.; Miedema, A. R. *Adv. Phys.* **1974**, *23*, 1.
(2) See the various articles in *Magneto-structural Correlations in Exchange Coupled Systems*, Willett, R. D.; Gatteschi, D.; Kahn, O., Eds.; NATO ASI Series; D. Reidel: Dordrecht, **1985**.
(3) For reviews on the percolation problem, see, e.g., Shante, V. K. S.; Kirkpatrick, S. *Adv. Phys.* **1971**, *20*, 325. Stauffer, D. *Phys. Rep.* **1979**, *54*, 1; Essam, J. W. *Rep. Progr. Phys.* **1980**, *43*, 883. Coniglio, A. In *Magnetic Phase Transitions*; Ausloos, M.; Elliott, R. J., Eds.; Springer, Berlin, **1983**; pp 195–222.
(4) Carlin, R. L. *J. Am. Chem. Soc.* **1961**, *83*, 3773.
(5) Wood, J. S.; de Boer, E.; Keijzers, C. P. *Inorg. Chem.* **1979**, *18*, 904.
(6) Wood, J. S.; Keijzers, C. P.; de Boer, E.; Buttafava, A. *Inorg. Chem.* **1980**, *19*, 2213.
(7) van Ingen Schenau, A. D.; Verschoor, G. C.; Romers, C. *Acta Crystallogr., Sect. B: Struct. Crystallogr. Cryst. Chem.* **1974**, *B30*, 1686.
(8) O'Connor, C. J.; Carlin, R. L. *Inorg. Chem.* **1975**, *14*, 291.
(9) Bergendahl, T. J.; Wood, J. S. *Inorg. Chem.* **1975**, *14*, 338.
(10) For an overview of the theory, the reader may consult the various volumes in the series: *Phase Transitions and Critical Phenomena*; Domb, C., Green, M. S., Ed. Academic: New York; 1972, Vol. 1, and succeeding volumes.
(11) van Ingen Schenau, A. D., Thesis, Leiden, **1976**.
(12) Taylor, D. *Aust. J. Chem.* **1978**, *31*, 713.
(13) Joung, K. O.; O'Connor, C. J.; Carlin, R. L. *J. Am. Chem. Soc.* **1977**, *99*, 7387.
(14) O'Connor, C. J.; Sinn, E.; Fariss, T. L.; Deaver, B. S., Jr. *J. Phys. Chem.* **1982**, *86*, 2369.
(15) Bartolome, J.; Algra, H. A.; de Jongh, L. J.; Carlin, R. L. *Physica B+C (Amsterdam)* **1978**, *B94*, 60.
(16) Carlin, R. L.; Joung, K. O.; Paduan Filho, A.; O'Connor, C. J.; Sinn, E. *J. Phys. C* **1979**, *12*, 293.
(17) Paduan Filho, A.; Sinn, E.; Chirico, R. D.; Carlin, R. L. *Inorg. Chem.* **1981**, *20*, 2688.
(18) O'Connor, C. J.; Sinn, E.; Carlin, R. L. *Inorg. Chem.* **1977**, *16*, 3314.
(19) Goodenough, J. B. *Phys. Rev.* **1955**, *100*, 564. Kanamori, J. *J. Phys. Chem. Solids* **1959**, *10*, 87. Ritter, R.; Jansen, L.; Lombardi, E. *Phys. Rev. B* **1973**, *8*, 2139. de Jongh, L. J.; Block, R. *Physica B+C (Amsterdam)* **1975**, *79B*, 568; van Kalkaren, G.; Schmidt, W. W.; Block, R. *Physica B+C (Amsterdam)* **1979**, *B97*, 315.
(20) Algra, H. A.; de Jongh, L. J.; Huiskamp, W. J.; Carlin, R. L. *Physica B+C (Amsterdam)* **1976**, *B83*, 71.
(21) Wood, J. S., private communication.
(22) Algra, H. A.; Bartolome, J.; de Jongh, L. J.; Carlin, R. L.; Reedijk, J. *Physica B+C (Amsterdam)* **1978**, *B93*, 114.
(23) Sams, J. R.; Tsin, T. B. *Inorg. Chem.* **1975**, *14*, 1573.
(24) Sams, J. R.; Tsin, T. B. *J. Chem. Phys.* **1975**, *62*, 734.
(25) Sams, J. R.; Tsin, T. B. *Chem. Phys.* **1976**, *15*, 209.
(26) Carlin, R. L.; O'Connor, C. J.; Bhatia, S. N. *J. Am. Chem. Soc.* **1976**, *98*, 685.
(27) Carlin, R. L.; O'Connor, C. J.; Bhatia, S. N. *J. Am. Chem. Soc.* **1976**, *98*, 3523.
(28) O'Connor, C. J. Thesis, University of Illinois at Chicago, Chicago, 1976.
(29) Smit, J. J.; de Jongh, L. J.; de Klerk, D.; Carlin, R. L.; O'Connor, C. J. *Physica B+C (Amsterdam)* **1977**, *B86–B88*, 1147.
(30) See the articles by L. J. de Jongh and by R. L. Carlin In *Magneto-structural Correlations in Exchange Coupled Systems*; Willett, R. D., Gatteschi, D., Kahn, O., Eds.; NATO ASI Series, D. Reidel: Dordrecht, 1985.
(31) Birdy, R. R.; Goodgame, M. *J. Chem. Soc., Dalton Trans.* **1977**, 461.
(32) Wood, J. S.; Keijzers, C. P.; de Boer, E. *Chem. Phys. Lett.* **1977**, *51*, 489.
(33) Algra, H. A.; de Jongh, L. J.; Carlin, R. L. *Physica B+C (Amsterdam)* **1978**, *93B*, 24; **1978**, *95B*, 224.
(34) Carlin, R. L.; van Duyneveldt, A. J. *Magnetic Properties of Transition Metal Compounds*; Springer-Verlag: New York, **1977**.
(35) de Jongh, L. J. *J. Appl. Phys.* **1978**, *49*, 1305; **1982**, *53*, 8018.
(36) Carlin, R. L.; van Duyneveldt, A. J. *Acc. Chem. Res.* **1980**, *13*, 231.
(37) Carlin, R. L. *Science* **1985**, *227*, 1291.
(38) Carlin, R. L. *Magnetochemistry*; Springer-Verlag: Berlin, Heidelberg, New York, Tokyo, 1986.
(39) Algra, H. A.; de Jongh, L. J.; Carlin, R. L. *Physica B+C (Amsterdam)* **1977**, *92B*, 258.
(40) Diederix, K. M.; Algra, H. A.; Groen, J. P.; Klaassen, T. O.; Poulis, N. J.; Carlin, R. L. *Phys. Lett. A* **1977**, *60A*, 247.
(41) Algra, H. A.; Bartolome, J.; Diederix, K. M.; de Jongh, L. J.; Carlin, R. L. *Physica B+C (Amsterdam)* **1977**, *B85*, 323.
(42) Bos, W. G.; Klaassen, T. O.; Poulis, N. J.; Carlin, R. L. *J. Magn. Magn. Mater.* **1980**, *15*, 464.
(43) Algra, H. A. Thesis, Leiden, **1977**.
(44) van der Bilt, A.; Joung, K. O.; Carlin, R. L.; de Jongh, L. J. *Phys. Rev. B: Condens. Matter* **1980**, *22*, 1259.
(45) van der Bilt, A.; Joung, K. O.; Carlin, R. L.; de Jongh, L. J. *Phys. Rev. B: Condens. Matter* **1981**, *24*, 445.
(46) Sinn, E.; O'Connor, C. J.; Joung, K. O.; Carlin, R. L. *Physica B+C (Amsterdam)* **1981**, *111B*, 141.
(47) Carlin, R. L.; van der Bilt, A.; Joung, K. O.; Northby, J.; Greidanus, F. J. A. M.; Huiskamp, W. J.; de Jongh, L. J. *Physica B+C (Amsterdam)* **1981**, *111B*, 147.
(48) Onsager, L. *Phys. Rev.* **1944**, *65*, 117.
(49) Tanaka, Y.; Uryû, N. *Phys. Rev. B: Condens. Matter* **1980**, *21*, 1994.
(50) Coyle, B. A.; Ibers, J. A. *Inorg. Chem.* **1970**, *9*, 767.
(51) Bencini, A.; Benelli, C.; Gatteschi, D.; Zanchini, C. *Inorg. Chem.* **1980**, *19*, 3839.
(52) Makinen, M. W.; Kuo, L. C.; Yim, M. B.; Wells, G. B.; Fukuyama, J. M.; Kim, J. E. *J. Am. Chem. Soc.* **1985**, *107*, 5245.
(53) Mennenga, G.; de Jongh, L. J.; Huiskamp, W. J.; Sinn, E.; Lambrecht, A.; Burriel, R.; Carlin, R. L. *J. Magn. Magn. Mater.* **1984**, *44*, 77.
(54) Myers, B. E.; Polgar, L. G.; Friedberg, S. A. *Phys. Rev. B: Condens. Matter* **1972**, *6*, 3488.
(55) Moriya, T. *Phys. Rev.* **1960**, *117*, 635.
(56) Algra, H. A.; Bartolome, J.; de Jongh, L. J.; O'Connor, C. J.; Carlin, R. L. *Physica B+C (Amsterdam)* **1978**, *93B*, 35.
(57) Diederix, K. M.; Groen, J. P.; Klaassen, T. O.; Poulis, N. J.; Carlin, R. L. *Physica B+C (Amsterdam)* **1979**, *97B*, 113.
(58) Bonner, J. C.; Fisher, M. E. *Phys. Rev.* **1964**, *A135*, 640.
(59) Navarro, R.; Algra, H. A.; de Jongh, L. J.; Carlin, R. L.; O'Connor, C. J. *Physica B+C (Amsterdam)* **1977**, *B86–B88*, 693.
(60) Bloembergen, P. *Physica B+C (Amsterdam)* **1977**, *B85*, 51.
(61) Reinen, D.; Krause, S. *Solid State Commun.* **1979**, *29*, 691.
(62) de Jongh, L. J. In *Recent Developments in Condensed Matter Physics*; Devreese, J. T., Ed.; Plenum: New York, **1981**; Vol. 1.
(63) (a) Burriel, R.; Lambrecht, A.; Carlin, R. L.; de Jongh, L. J., unpublished. (b) Navarro, R., to be published.
(64) Blöte, H. W. J. *J. Appl. Phys.* **1979**, *50*, 1825.
(65) de Jongh, L. J.; Mennenga, G.; Coniglio, A. *Physica B + C (Amsterdam)* **1985**, *B132*, 100.
(66) de Jongh, L. J. In *Magnetic Phase Transitions*; Ausloos, M.; Elliott, R. J., Eds.; Springer-Verlag: Berlin, **1983**.
(67) Harris, A. B.; Kirkpatrick, S. *Phys. Rev. B: Condens. Matter* **1977**, *16*, 542.
(68) Algra, H. A.; de Jongh, L. J.; Huiskamp, W. J.; Reedijk, J. *Physica B+C (Amsterdam)* **1977**, *B86–B88*, 737.
(69) Algra, H. A.; de Jongh, L. J.; Reedijk, J. *Phys. Rev. Lett.* **1979**, *42*, 606.
(70) Burriel, R.; Lambrecht, A.; Carlin, R. L.; de Jongh, L. J., to be published.
(71) Mennenga, G.; de Jongh, L. J.; Huiskamp, W. J.; Reedijk, J. *J. Magn. Magn. Mater.* **1984**, *43*, 3.
(72) Skal, A.; Shklovskii, B. I. *Sov. Phys. Semicond. (Engl. Transl.)* **1975**, *8*, 1029.
(73) de Gennes, P. G. *J. Phys. Lett. (Paris)* **1976**, *37*, L1.
(74) Mennenga, G.; de Jongh, L. J.; Huiskamp, W. J.; Reedijk, J. *J. Magn. Magn. Mater.* **1984**, *43*, 13.
(75) Al-Karaghouli, A. R.; Wood, J. S. *Inorg. Chem.* **1979**, *18*, 1177.
(76) Carlin, R. L.; Burriel, R.; Mennenga, G.; de Jongh, L. J., to be published.
(77) Carlin, R. L.; Burriel, R.; Pons, J.; Casabo, J. *Inorg. Chem.* **1983**, *22*, 2832.
(78) Cotton, S. A.; Gibson, J. F. *J. Chem. Soc. (A)* **1970**, 2105.
(79) Schäfer, H. L.; Morrow, J. C.; Smith, H. M. *J. Chem. Phys.* **1956**, *42*, 504; Sager, R. S.; Williams, R. J.; Watson, W. H. *Inorg. Chem.* **1967**, *6*, 951. Watson, W. H. *Inorg. Chem.* **1969**, *8*, 1879. Kidd, M. R.; Watson, W. H. *Inorg. Chem.* **1969**, *8*, 1886.
(80) McGregor, K. T.; Barnes, J. A.; Hatfield, W. E. *J. Am. Chem. Soc.* **1973**, *95*, 7993.
(81) Scavnicar, S.; Matkovic, B. *Acta Crystallogr.* **1969**, *B25*, 2046.
(82) Hatfield, W. E. *Inorg. Chem.* **1983**, *22*, 833.
(83) Carlin, R. L.; Burriel, R.; Cornelisse, R. M.; van Duyneveldt, A. J. *Inorg. Chem.* **1983**, *22*, 831.